Journal of Molecular Liquids 389 (2023) 122882

Contents lists available at ScienceDirect

Journal of Molecular Liquids

journal homepage: www.elsevier.com/locate/molliq

Multiple evidences for molecular level heterogeneity in a non-ionic biocatalytic deep eutectic solvent

Tanmoy Khan [a,1], Ejaj Tarif [a,1], Yuto Awano [b], Lou Serafin Lozada [b], Nilimesh Das [a], Keisuke Tominaga [b,c], Pratik Sen [a,*]

[a] Department of Chemistry, Indian Institute of Technology Kanpur, Kanpur 208 016, UP, India
[b] Department of Chemistry, Graduate School for Science, Kobe University, Nada, Kobe 657-8501, Japan
[c] Molecular Photoscience Rersearch Center, Kobe University, Nada, Kobe 657-8501, Japan

ARTICLE INFO

Keywords:
Spatial heterogeneity
Dynamic heterogeneity
Deep eutectic solvent
Solvation dynamics
Fluorescence anisotropy
Translational dynamics
Viscosity decoupling

ABSTRACT

Deep eutectic solvents (DESs) are new-generation solvents with exquisite and tuneable properties. Molecular-level heterogeneity has been identified as an intriguing feature of such solvents. Herein, we examined the spatio-temporal heterogeneity of a potential non-ionic biocatalytic DES, acetamide/urea/sorbitol (0.5Ac/0.3Ur/0.2Sor), and compared the result with corresponding binary acetamide/urea (0.6Ac/0.4Ur) DES, and another related non-ionic ternary DES (0.55Ac/0.36Ur/0.09PEG). The effect of the addition of a third component on the spatio-temporal heterogeneity of a DES was investigated. The excitation wavelength-dependent emission measurement suggests an induction of spatial heterogeneity in acetamide/urea/sorbitol compared to spatially homogenous acetamide/urea and acetamide/urea/PEG. The dynamic heterogeneity measurements in terms of solvation dynamics, dielectric relaxation, and rotational/translational diffusion indicate a length and timescale dependency. Overall, acetamide/urea/sorbitol is found to be dynamically more heterogenous than the other two related DESs.

1. Introduction

Structure and dynamics control chemistry and biology. Modern science has identified molecular level heterogeneity as one of the intriguing aspects of structure and dynamics [1–4]. The heterogeneity of a medium is relative to the observation dimension. For the sub-atomic length scale of observation, every system will appear to be heterogeneous and with a bigger dimension of observation this heterogeneity will tend to smear out as unobservable.

In the literature, one would invariably encounter two terms, spatial and dynamic heterogeneity, which are often used interchangeably [5,6]. Heterogeneity mainly originates from the presence of different interactions in terms of spatial arrangement or relaxation rates. The first one is defined as spatial heterogeneity, and the latter is described as dynamic heterogeneity [5–7].

The molecular-level picture of heterogeneity both in terms of structure and dynamics mainly comes from studies of glass-forming liquid that shows viscosity decoupled relaxation rates near glass transition temperature (T_g) due to microdomain formation [8–12]. These locally preferred clusters facilitate local structural relaxation but do not facilitate the relaxation of the entire system [11,13,14]. Even if the Stokes-Einstein (SE) relationship is locally satisfied within these microdomains and bulk, their spatial averages might indicate a deviation from the SE relationship due to preferential sampling from the microdomains [15]. A unique breakthrough in this field comes when viscosity decoupled relaxation rates were identified for polar and non-polar liquids at a much higher temperature than the T_g [16]. In the case of polar and H-bonded solvents, minimal decoupling was observed [16]. Consequent research proved that such dynamic heterogeneity, even at ambient room temperature might well be a common phenomenon for ILs and DESs [17–25].

DESs are already touted as the next game-changer in various fields of chemistry and biology owing to their green character, easy and atom-economic synthesis, exceptional tunability, biocompatibility, low volatility, etc. [26–29]. Many recent reviews are available that summarise various uses of DES in many different fields [26,27,30–35]. However,

* Corresponding author.
E-mail address: psen@iitk.ac.in (P. Sen).
[1] Authors contributed equally.

https://doi.org/10.1016/j.molliq.2023.122882
Received 5 April 2023; Received in revised form 18 August 2023; Accepted 19 August 2023
Available online 21 August 2023

from the viewpoint of a physical chemist, we are more interested in the molecular level insight of such systems. Most of the works in this direction are with ionic DESs. Only a handful of reports are available deciphering the structure and dynamics of non-ionic DESs [36–39].

Biswas group has explored various acetamide-based ionic DESs, and they showed the presence of substantial dynamic and spatial heterogeneity in these systems [17,18,40–44]. Replacement of electrolytes by the non-ionic urea makes the system almost homogeneous, both in relaxation rates and spatial arrangement [19,38,45]. However, this DES is not liquid at room temperature, thus limiting its use. Recently, a third component (PEG-300) is added to the acetamide/urea DES to lower its freezing point down to 303 K [20]. Moreover, this system is spatially homogeneous, but its rotational relaxation shows considerable viscosity decoupling [20].

In this context, herein we have chosen sorbitol as the third component, which itself is solid. The ternary 0.5Ac/0.3Ur/0.2Sor DES is liquid even at 253 K, making it an interesting non-ionic DES for practical applications [46]. We have already shown the positive effect of 0.5Ac/0.3Ur/0.2Sor DES on protein structure and activity [47]. Herein we employed steady-state/time-resolved fluorescence and fluorescence correlation spectroscopy covering a broad range of lengths and time scales to decipher the microscopic heterogeneity of this DES. We have also used dielectric relaxation spectroscopy to understand the inherent medium dynamics and associated heterogeneity of the system. Our results demonstrate that the system is highly heterogenous both spatially and dynamically, and the extent of heterogeneity depends on the length scale of the measurement. We also compared the heterogeneity of this DES with the corresponding binary acetamide/urea (0.6Ac/0.4Ur) DES, and another similar non-ionic ternary DES (0.55Ac/0.36Ur/0.09PEG), and investigated the effect of the addition of a third component on the spatio-temporal heterogeneity.

2. Materials and methods

2.1. Materials

Acetamide (> 99%), urea (> 99%), sorbitol (> 98%), and rhodamine 6G (R6G) (dye content 99.0%) were purchased from Sigma-Aldrich; PEG-300 was purchased from TCI; coumarin 153 (C153) was purchased from exciton. Acetamide and urea were dried overnight under a vacuum at room temperature before use. Sorbitol, R6G, and C153 were used without further purification.

2.2. Acetamide-Urea-Sorbitol DES preparation

Acetamide/urea/sorbitol DES was prepared by mixing the appropriate amounts (0.5 Ac + 0.3 Ur + 0.2 Sor) of the constituents in a sealed container and slowly heating to 75 °C while stirring.[46]. After one hour a clear solution of DES was obtained, which was used for all the experiments.

2.3. Acetamide-Urea-PEG DES preparation

Acetamide, urea and PEG-300 with a molar ratio of 0.55:0.36:0.09 was used to form the (0.55Ac/0.36Ur/0.09PEG) DES following the published procedure [20]. This DES is not liquid at room temperature (at 298 K) and becomes solid, however, at the experimental temperature range, a clear liquid state was observed.

2.4. Viscosity measurement

Dynamic viscosity of the sample was measured with a rolling-ball viscometer (Lovis 2000 M, Anton Paar, Austria) with an inbuilt temperature controller.

2.5. Water content measurement

To determine the water content of DESs, we performed Karl Fisher titration (KAFI LABINDIA KF Titrator). For freshly prepared (from overnight vacuum dried constituents) 0.5Ac/0.3Ur/0.2Sor DES, the water content is measured to be 0.3 % (w/w), whereas for 0.55Ac/0.36Ur/0.09PEG DES the water content is found to be 0.4 % (w/w).

2.6. Sample preparation for spectroscopic measurements

Samples for spectroscopic measurements were prepared by taking a known amount of ethanol solution of the dye (C153 or R6G) in a cuvette/glass vial. Ethanol was dried in a vacuum oven so that no trace of ethanol was present in the cuvette. After ethanol was evaporated from the container, an appropriate amount of DES was added and sealed immediately using Teflon to make the dye-DES solution. For the steady-state and time-resolved fluorescence measurements, C153 was added such that the solution absorbance lies between 0.1 and 0.2. For the FCS measurement, R6G concentration was kept around 30–40 nM.

2.7. Steady-state measurements

We performed the steady-state absorption measurement on a commercial double-beam UV–Vis spectrophotometer (UV-2450, Shimadzu, Japan). The emission measurements were performed on a commercial fluorimeter (FluoroMax-4, Jobin-Yvon, USA). In all experiments a 10 mm pathlength cuvette was used. The temperature was controlled by an external temperature controller connected to the spectrophotometer and fluorimeter with an accuracy of 0.5 °C. Emission maxima were estimated by taking the first derivative of the spectrum. For REES measurement, the emission spectra were collected by exciting the sample up to 5% absorbance value of that at the absorption maximum.

2.8. Time-resolved fluorescence measurements

Fluorescence transients of C153 in DES were measured using a picosecond time-correlated single-photon counting (TCSPC) set-up (LifeSpec-II, Edinburgh Instruments, UK) under the magic angle (54.7°) condition. The excitation wavelength was 405 nm. Other details of this setup are described elsewhere [37,48,49]. The instrument response function (IRF) of the TCSPC set-up is ~130 ps. Average excited state lifetimes, $\langle \tau_{life} \rangle$, was estimated from the normalized magic angle fluorescence transient, $I(t)$, collected at the emission peak wavelengths using equation (1).

$$I(t) = \sum_i a_i e^{\frac{-t}{\tau_i}}, \langle \tau_{life} \rangle = \sum_i a_i \tau_i, \quad \text{with} \quad \sum_i a_i = 1 \tag{1}$$

2.9. Solvation dynamics measurement

Solvation dynamics were measured using the time-dependent fluorescence Stokes shift (TDFSS) method.[37,50] About 16 to 18 fluorescence transients at several wavelengths across the steady-state emission spectrum of C153 dissolved in 0.5Ac/0.3Ur/0.2Sor DES were recorded, and then time-resolved emission spectra (TRES) were reconstructed following the established protocol.[50,51] Subsequently, the normalized solvation response function was constructed as follows [52]

$$S(t) = \frac{\nu(t) - \nu(\infty)}{\nu(0) - \nu(\infty)} \tag{2}$$

where $\nu(t)$, $\nu(0)$, and $\nu(\infty)$ represent the emission maxima at time t, 0, and ∞, respectively. The average solvation time, $\langle \tau_s \rangle$, was obtained by fitting $S(t)$ to a multi-exponential function (Eq. (3) and taking the average of the decay time components as $\langle \tau_s \rangle = \sum_i b_i \tau_{si}$, where $\sum_i b_i = 1$.

$$S(t) = \sum_i b_i e^{\frac{-t}{\tau_{Si}}} \quad (3)$$

2.10. Dielectric relaxation measurement

Dielectric relaxation measurements were performed using a vector network analyzer E5071C (Agilent Technologies) combined with a dielectric probe kit 85070E (Agilent Technologies). The details of the setup and analysis can be found elsewhere [53,54] and also given in the supporting information (section S1 of the Supplementary Material).

2.11. Fluorescence anisotropy measurement

Time-resolved fluorescence anisotropy measurements were performed by taking the fluorescence transients at the parallel ($I_{||}$) and perpendicular ($I_{\perp}$) polarization with respect to the polarization of the excitation light, at the steady-state emission maximum of C153. Dynamic anisotropy was calculated as [51]

$$r(t) = \frac{I_{||}(t) - GI_{\perp}(t)}{I_{||}(t) + 2GI_{\perp}(t)} \quad (4)$$

Here, G is the G-factor (ratio of I_{HV} and I_{HH}) of the instrument. The anisotropy decay was then fitted with a bi-exponential function with associated anisotropy as

$$r(t) = c_1 e^{\frac{-t}{\tau_{r1}}} + c_2 e^{\frac{-t}{\tau_{r2}}} \quad (5)$$

The average reorientation time $\langle \tau_r \rangle$ was obtained by taking the average of the decay time components as $\langle \tau_r \rangle = \frac{c_1\tau_{r1} + c_2\tau_{r2}}{c_1 + c_2}$.

2.12. Fluorescence correlation spectroscopy (FCS) measurement

We performed the fluorescence correlation spectroscopic (FCS) measurements on an instrument built in our laboratory. The details can be found in our previous publications [47,55–57] and section S2 of the Supplementary Material. For a single component system, assuming Gaussian detection volume, fluorescence intensity autocorrelation function (ACF) can be written as [51,58]

$$G(\tau) = \frac{1}{N}\left(1 + \frac{\tau}{\tau_D}\right)^{-1}\left(1 + \frac{\tau}{\omega^2\tau_D}\right)^{-1/2} \quad (6)$$

In the above equation, N is the number of particles in the observation volume, τ_D is the diffusion time, and ω is the aspect ratio of the observation volume, which is given by, ω = l/r and l and r are the longitudinal and transverse radius of the 3D Gaussian volume respectively. The excitation volume of the FCS setup was calibrated by measuring several fluorescence intensity autocorrelation curves of rhodamine 6G (R6G) with varying concentrations in water and globally fitted them to determine the value of ω. While calibrating the value of ω, the diffusion coefficient of R6G in water was taken to be $D_t = 4.14 \times 10^{-6}$ cm^2 s^{-1} [59]. For a particular set of experiments, 'ω' was fixed during fitting. For anomalous diffusion, the autocorrelation function can be written as [58]

$$G(\tau) = \frac{1}{N}\left(1 + \left(\frac{\tau}{\tau_D}\right)^{\alpha}\right)^{-1}\left(1 + \frac{1}{\omega^2}\left(\frac{\tau}{\tau_D}\right)^{\alpha}\right)^{-1/2} \quad (7)$$

where α is the anomalous coefficient. α is a measure of the extent of deviation from normal diffusion. The diffusion is referred to as sub-diffusion for $0 < \alpha < 1$, normal diffusion for $\alpha = 1$, and super diffusion for $\alpha > 1$. For more than one-particle diffusing normally (i.e. $\alpha = 1$), the ACF can be written as [58]

$$G(\tau) = \frac{1}{\left(\sum_i N_i\right)^2}\sum_i N_i D_i(\tau); D_i(\tau) = \left(1 + \frac{\tau}{\tau_{D_i}}\right)^{-1}\left(1 + w^2\frac{\tau}{\tau_{D_i}}\right)^{-\frac{1}{2}} \quad (8)$$

While taking temperature-dependent FCS measurements, at least 45 min of equilibration time has been given before taking the data after the system reaches the desired temperature.

3. Results and discussion

3.1. Steady-state measurements

At 298 K, the absorption and emission maxima of C153 in 0.5Ac/0.3Ur/0.2Sor non-ionic DES were measured to be 433.7 nm (23057.4 cm^{-1}) and 534.5 nm (18709.1 cm^{-1}), respectively. Interestingly, with an increase in the temperature (298 K to 343 K) we observed a very small blue shift of ~1.5 nm in the absorption spectra (Fig. 1a and section S3 of Supplementary Material). Such a surprising blue shift with increasing temperature might be due to decreasing dielectric constant of the medium with increasing temperature [60,61]. Similar observations were also made with other ionic liquids and DESs [17]. In the emission spectrum, we observed a red shift of 9.5 nm with the increase in the temperature (298 K to 343 K) (Fig. 1b, section S3 of Supplementary Material). The observation could be explained as follows. The medium here is highly viscous (Table 1). At low temperatures, emission originates from an incomplete solvated state. With an increase in the temperature the emission is expected to originate from a more solvated state (red shifted), which is the origin of the red edge excitation shift (REES) [62,63]. Furthermore, a competition between solvation time and probe lifetime critically controls the detection of heterogeneity through REES [51,64,65].

We measured the excitation wavelength (λ_{ex}) dependent emission maxima (λ_{em}) of C153 dissolved in 0.5Ac/0.3Ur/0.2Sor DES and observed a REES of 10 nm (346.3 cm^{-1}) at 303 K (Fig. 1c and section S4 of Supplementary Material). However, as the transition did not get saturated, it was difficult to comment on the actual value of REES. Azumi *et al.* suggested that the absolute value of REES can be obtained by taking the emission spectra at very high temperatures where all the emissions are expected to originate from a completely solvated state. [66,67] In this way, a REES of ~11.5 nm (~400 cm^{-1}) was calculated for C153 in 0.5Ac/0.3Ur/0.2Sor DES that indicated the presence of moderate spatial heterogeneity, with respect to the lifetime of C153 at 303 K (Section S5 and S6 of the Supplementary Material for the lifetime of the probe at various temperature).

3.2. Solvation dynamics study

We measured the solvent response of C153 in 0.5Ac/0.3Ur/0.2Sor DES at different temperatures using the time-dependent fluorescent Stokes shift (TDFSS) method. Time-resolved emission spectra (TRES) and solvent response function (S(t)) was constructed (Section S7 of the Supplementary Material for the raw data). TRES in two representative temperatures are shown in Fig. 2a and 2b. The calculated $S(t)$ at different temperatures along with the bi-exponential fitting are shown in Fig. 2c, and the parameters are tabulated in Table 1.

The average solvation time of 0.5Ac/0.3Ur/0.2Sor DES at 318 K was found to be 430 ps, which decreases to 156 ps at 343 K. The solvent responses are characterized by a fast component (~150–70 ps) with 65–85 % contribution and a relatively slower component (~950–640 ps) with 15–35% contribution. The amplitude of the fast component increases, whereas the slow component decreases with an increase in temperature. The missing percent, calculated from the Fee-Maronceli method [68], was around 40–50 % for temperature values. Previously, DESs were also reported with a missing percentage in this range or higher using the picosecond TDFSS method [64,65,69]. The estimated large missing percentage is probably due to the presence of ultrafast solvation component in 0.5Ac/0.3Ur/0.2Sor DES. Measurement with better time resolution may catch the information that was missed here.

It can be observed from Fig. 2c that with an increase in temperature, the temporal decay of solvent response function becomes faster, which may be thought to be solely associated with the viscosity drop of the medium. However, solvation time decreases about 2.7 times on raising

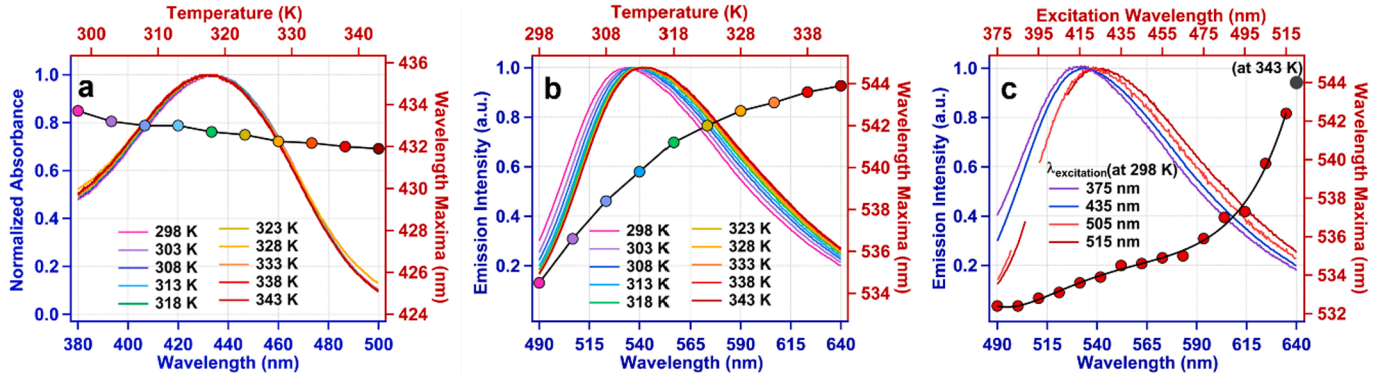

Fig. 1. Steady-state (a) absorption and (b) emission spectra of C153 dissolved in 0.5Ac/0.3Ur/0.2Sor DES. (c) Excitation wavelength-dependent emission of C153 in this DES at 298 K. Here axes are colour-coded. Similar colour axes imply the respective X and Y axis for the data plotted. In the case of excitation wavelength-dependent emission, the red data points are plotted concerning red axes.

Table 1
Bi-exponential fitting parameters of solvent response function $S(t)$ of 0.5Ac/0.3Ur/0.2Sor DES and its viscosities at different temperatures. Note that SS means stokes shift.

Temp (K)	b_1	τ_{S1}(ps)	b_2	τ_{S2}(ps)	$\langle\tau_S\rangle$(ps)	SS (cm^{-1})	η (cP)	% missed
318	0.65 ± 0.02	150 ± 40	0.35 ± 0.02	950 ± 40	430 ± 50	670 ± 70	482.3 ± 9	47
323	0.67 ± 0.02	100 ± 20	0.33 ± 0.02	690 ± 30	280 ± 30	760 ± 70	307.2 ± 5	41
328	0.75 ± 0.02	110 ± 20	0.25 ± 0.02	730 ± 30	265 ± 35	670 ± 60	202.0 ± 8	51
333	0.77 ± 0.02	80 ± 10	0.23 ± 0.02	670 ± 20	215 ± 25	770 ± 80	141.0 ± 8	44
338	0.83 ± 0.02	90 ± 10	0.17 ± 0.02	670 ± 10	190 ± 20	650 ± 50	90.3 ± 6	53
343	0.85 ± 0.02	70 ± 10	0.15 ± 0.02	640 ± 10	155 ± 20	650 ± 60	66.3 ± 8	54

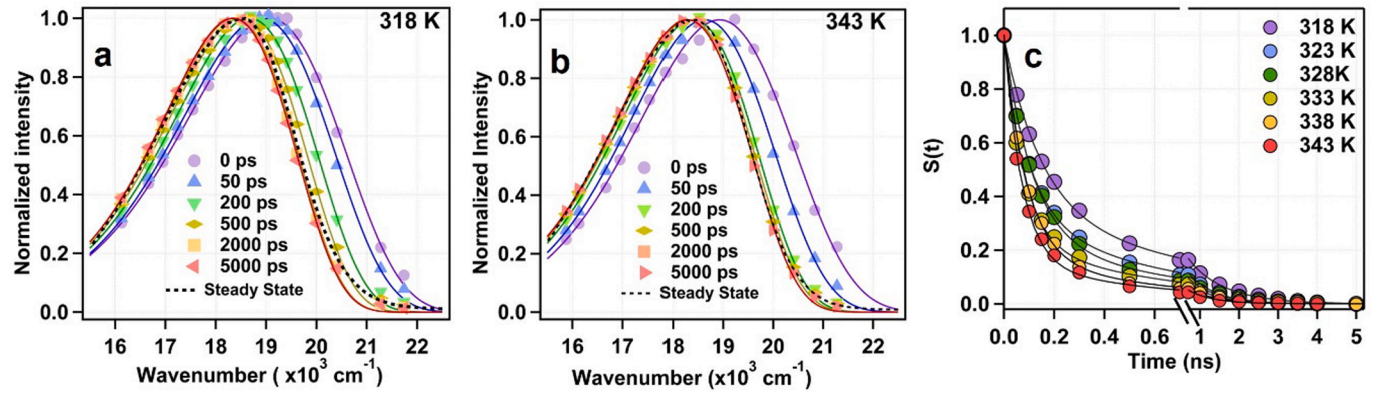

Fig. 2. Representative time-resolved emission spectra at (a) 318 K and (b) 343 K. Emission spectra at various times are colour-coded and mentioned in the respective plots. Each steady-state emission spectra at that temperature exciting at the same wavelength as the time-resolved study are represented with a black dashed line. (c) Solvent response functions at different temperatures. Solid lines represent fittings by Eq. (3).

the temperature from 318 K to 343 K, while viscosity decreases ~7.3 times. It hints that the medium viscosity does not solely control the solvation of C153 in 0.5Ac/0.3Ur/0.2Sor DES. To see the relationship between medium viscosity and solvation time, we plotted the average solvation time as a function of temperature-reduced viscosity in a double logarithmic fashion, and the slope (p-value) is 0.45 (Fig. 3a). If simple diffusion controls the solvation, then a near unity p-value should have been observed. That is the case when Jin *et al.* examined the solvation dynamics of C153 in normal H-bonded solvents and 21 room-temperature ionic liquids [70]. In the present case, a pronounced fractional viscosity dependence indicates the existence of dynamic heterogeneity in the medium. We also estimated the activation energy (E_s^a) associated with the solvation dynamics as 33.27 kJ mol^{-1} (Fig. 3b), which is ~2.2 times less than the activation energy of viscous flow (E_η^a = 72.35 kJ mol^{-1}) (Fig. 3c). This result also shows the deviation of solvation dynamics from the medium viscosity.

3.3. Dielectric relaxation study

Dielectric relaxation spectroscopy (DRS) is an extensively used technique to measure the frequency-dependent dielectric response of a dipolar system by applying an external electric field. The interaction of the electric field with a dipolar system in the broad frequency range gives information about the collective reorientation dynamics. DRS is a non-invasive technique and complements fluorescence spectroscopic results in a better way. We have performed temperature-dependent (318–343 K) DRS measurements to collect information about the relaxation dynamics of the dipolar constituents of 0.5Ac/0.3Ur/0.2Sor DES system in the GHz region.

As representative data, we show the real (ε') and imaginary (ε'') parts of the complex dielectric spectra at 343 K with a 2-Debye fitting in Fig. 4a. All the temperature dependent dielectric spectra along with their respective 2-Debye fitting lines are given in the supporting

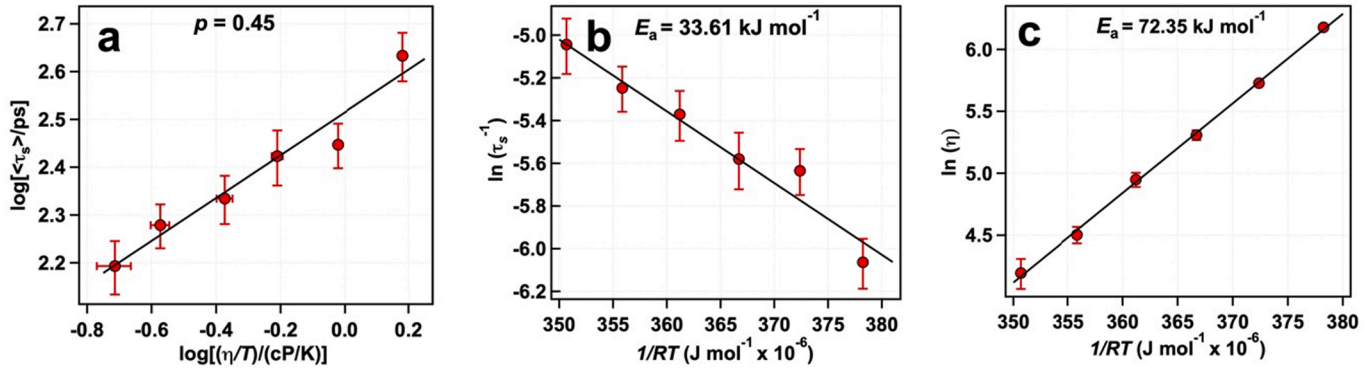

Fig. 3. (a) Log-log plot of average solvation time ($\langle\tau_s\rangle$) vs temperature-reduced viscosity, $\left(\frac{\eta}{T}\right)$, with a linear fit (solid black line). (b) Arrhenius plot of average solvation time and (c) activation energy of viscous flow plot.

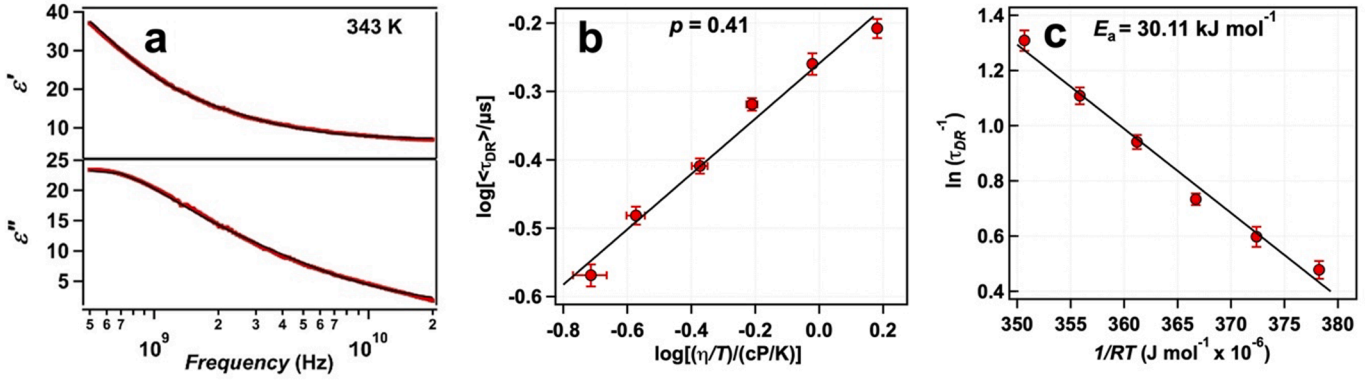

Fig. 4. (a) Representative real (ε') and imaginary (ε'') parts of the complex dielectric spectra of 0.5Ac/0.3Ur/0.2Sor DES at 343 K with 2-Debye fit (solid black lines). (b) Log-log plot of average DR time $\langle\tau_{DR}\rangle$ vs temperature-reduced viscosity, $\left(\frac{\eta}{T}\right)$ with the linear fit represented by the solid black line. (c) Arrhenius plot of average DR time.

information (Section S8 of Supplementary Material). The necessary parameters obtained are summarized in Table 2. Two-time components are obtained from the fitting, one in the range of sub-nanosecond (τ_1) and another in the picosecond (τ_2). As expected, the long-time component dominates the relaxation (amplitude ~90%) and decreases with increasing temperature. The short-time component is found to be temperature insensitive. The average DR time also decreases with temperature, and to explore the relationship with the medium viscosity we plotted it against temperature-reduced viscosity in a log-log graph in Fig. 4b. The obtained p-value 0.41 indicates substantial dynamic heterogeneity. The estimated activation energy (E^a_{DR}) associated with the dielectric relaxation dynamics is 30.1 kJ mol^{-1} (Fig. 4c), which is ~2.4 times less than the activation energy of viscosity (E^a_η = 72.3 kJ mol^{-1}). This difference in activation energy associated with reorientational dynamics (DR dynamics) and viscosity is reflected in the p-value as well.

Table 2
Temperature-dependent fitting parameters obtained from simultaneous 2-Debye fits to real (ε') and imaginary (ε'') components of the measured DR spectra for 0.5Ac/0.3Ur/0.2Sor DES.

Temp (K)	$\Delta\varepsilon_1$	τ_1(ns)	$\Delta\varepsilon_2$	τ_2(ns)	$\langle\tau_{DR}\rangle$(ns)	ε_∞
318	33.6 ± 0.19	0.69 ± 0.02	3.9 ± 0.16	0.053 ± 0.002	0.62 ± 0.02	6.37
323	38.5 ± 0.08	0.61 ± 0.02	4.5 ± 0.12	0.053 ± 0.002	0.55 ± 0.02	6.54
328	41.7 ± 0.08	0.53 ± 0.01	5.2 ± 0.08	0.053 ± 0.001	0.48 ± 0.01	6.68
333	43.8 ± 0.25	0.44 ± 0.01	6.0 ± 0.08	0.053 ± 0.001	0.39 ± 0.01	6.89
338	44.2 ± 0.26	0.37 ± 0.01	6.9 ± 0.09	0.053 ± 0.001	0.33 ± 0.01	7.10
343	44.0 ± 0.12	0.31 ± 0.01	7.7 ± 0.09	0.052 ± 0.001	0.27 ± 0.01	7.19

3.4. Rotational dynamics study

Temperature ($318K \leq T \leq 343K$) dependent fluorescence anisotropy decays ($r(t)$) of C153 in 0.5Ac/0.3Ur/0.2Sor DES along with its fitting line (Equation (5) with a bi-exponential function are depicted in Fig. 5a (Section S9 of the Supplementary Material for the raw data), and the fitting parameters are tabulated in Table 3. $r(t)$ is characterized by a fast sub-nanosecond time component and a dominant slow component (~90%) of a few nanoseconds. With an increase in the temperature, both the amplitude and the component of the faster time constant increases, while, the slower time component and its amplitude decreases. As a result, with increasing temperature, the average rotational time ($<\tau_r>$) decreases from ~5 ns to ~1.5 ns from 318 K to 343 K.

We plotted the average rotational time $\langle\tau_r\rangle$ as a function of temperature-reduced viscosity (η/T) in log–log fashion (Fig. 5b) to identify how extensively the medium viscosity controls the solute (C153) rotation in 0.5Ac/0.3Ur/0.2Sor DES. Interestingly, we found a substantial decoupling of rotational motion from the viscosity with $p \approx 0.61$. Such fractional viscosity dependence might arise from various factors like the non-spherical shape of the probe molecule, the non-continuum nature of the solvent medium, specific interaction between solvent and solute, and non-Brownian motion like large angle jumps and inertia-driven motion especially in a viscous liquid, apart from the dynamical heterogeneous characteristics of the media. Normally, the

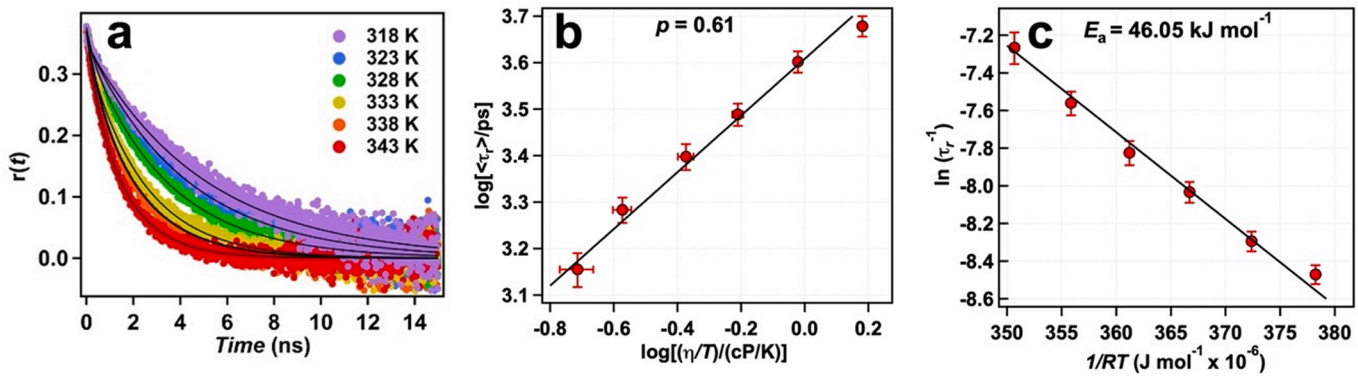

Fig. 5. (a) Fluorescence anisotropy decays of C153 in 0.5Ac/0.3Ur/0.2Sor DES at different temperatures with a bi-exponential fit (solid black lines). (b) Log-log plot of average rotational diffusion time (τ_r) vs temperature-reduced viscosity (η/T) with the linear fit represented by a solid black line. (c) Arrhenius plot of average probe rotational time.

Table 3
Biexponential fitting parameters of fluorescence anisotropy decays *r(t)* in 0.5Ac/0.3Ur/0.2Sor DES at different temperatures.

Temp (K)	c_1	τ_{r_1} (ps)	c_2	τ_{r_2} (ps)	$\langle\tau_r\rangle$ (ps)
318	0.04 ± 0.02	110 ± 40	0.96 ± 0.02	4960 ± 150	4770 ± 240
323	0.04 ± 0.02	110 ± 30	0.96 ± 0.02	4160 ± 130	4000 ± 210
328	0.09 ± 0.02	290 ± 60	0.91 ± 0.02	3360 ± 110	3080 ± 170
333	0.08 ± 0.02	220 ± 40	0.92 ± 0.02	2700 ± 120	2500 ± 160
338	0.16 ± 0.02	580 ± 30	0.84 ± 0.02	2170 ± 100	1920 ± 120
343	0.20 ± 0.02	610 ± 20	0.80 ± 0.02	1640 ± 120	1430 ± 120

formation of DES is explained by strong H-bond formation between its constituents [26,27]. In the present case, where all the constituents are non-ionic, the solvent could be identified as an H-bonded solvent. For typical H-bonding solvents, Horng *et al.* demonstrated that the rotation of C153 exhibits a power-law dependency on the viscosity with $p = 0.96$ [16]. This study eliminates the possibility of non-sphericity and specific interaction induced break down on SED relationship. In another study, Jin *et al.* demonstrated that there is no specific interaction between C153 and 21 ionic liquids [70]. Using these data, Guchhait *et al.* calculated a near unity *p*-value of the system [44]. This observation somewhat eliminates the probability of fractional dependence of viscous liquids (like in our case) due to non-Brownian motion. Although it is very difficult to ascertain how much of the decoupling between average rotational time and viscosity originates from the violation of the assumptions stated in the SED relationship or from the underlying microscopic heterogeneity, the preceding discussion strongly hints toward the presence of dynamic heterogeneity in corresponding length (nm) and time (ns) scale.

The estimated activation energy (E_r^a) associated with rotational dynamics of C153 is ~46 kJ mol^{-1} (Fig. 5c), which is ~ 1.6 times smaller than the activation energy (E_η^a) associated with the viscous flow of the system. This observation also supports that the fractional viscosity dependency of rotational dynamics leads to the dynamic heterogeneity of the medium.

3.5. Translational dynamics study

We measured the fluorescence intensity autocorrelation function of R6G in 0.5Ac/0.3Ur/0.2Sor DES at various temperatures (318 K to 343 K) (Fig. 6) to investigate translational diffusion dynamics through FCS

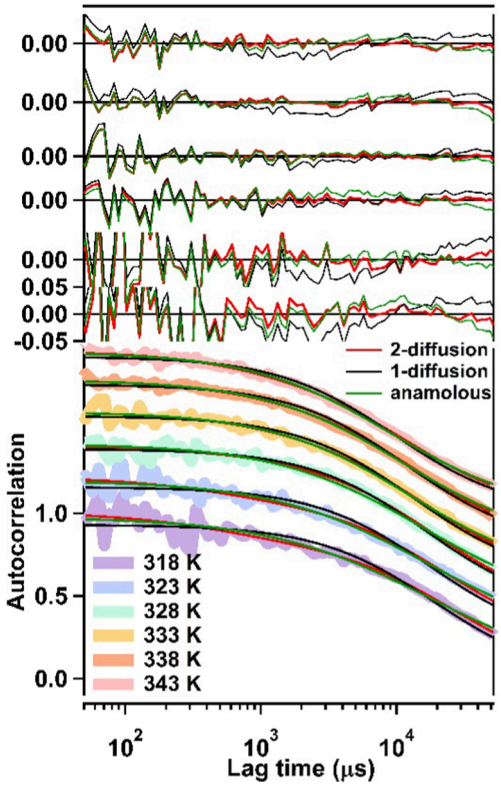

Fig. 6. Translational dynamics via single molecular level FCS. Normalized fluorescence intensity autocorrelation curve of R6G in 0.5Ac/0.3Ur/0.2Sor DES at different temperatures. Fitting lines using equations (6), 7, and 8 are shown by solid black, green, and red lines, respectively. The respective residuals of fittings are also shown with the same colours.

[58,71]. To begin with, we fitted our data by simple Stokes-Einstein diffusion (normal diffusion model with one diffusion coefficient represented using equation (6). The fitting quality is found to be reasonably good, and the fitting parameters are tabulated in section S10 of the Supplementary Material. In this case, the observed *p*-value from the log-log plot of the average translational diffusion time ($\langle\tau_D\rangle$) and temperature-reduced viscosity (see section S11 of Supplementary Material) is 0.33, which is quite low compared to the *p*-value obtained from solvation dynamics, dielectric relaxation, and fluorescence anisotropy studies. This suggests the existence of higher decoupling in translational dynamics in 0.5Ac/0.3Ur/0.2Sor DES.

One self-contradicting point is that the fitting parameters that are

used in *p*-value calculation are obtained from normal diffusion, yet the *p*-value showed a significant deviation from normal diffusion. A close inspection of the fitting lines and fit residues reveals that the fitting is not perfect. Generally, diffusion in a complex environment is described by anomalous diffusion. For such diffusion, autocorrelation traces should be described by equation 7. The fitting results with anomalous diffusion are shown in section S10 of the Supplementary Material. As can be seen, the introduction of the anomalous exponent does not significantly improve the quality of the fitting (Fig. 6). The values of anomalous exponent are also close to 1, hinting that the diffusion is primarily normal SE diffusion. The *p*-value obtained in this way (0.32, section S11 of Supplementary Material) is also very similar to what was obtained using the normal diffusion equation (0.33). In the case of heterogeneous distribution, a probe can show multi-diffusion phenomena. This is not rare in complex liquid systems.[41,72–74] Inspired by this fact, we fitted our autocorrelation functions with a two-diffusion equation (equation (8) with $i = 2$) (see Fig. 6 for the fitting result and Table 4 for the fitting parameters). It is clear that the fitting quality improved greatly. The slower diffusion component is very much like what we obtained from the fitting by one diffusion equation and shows somewhat similar temperature dependence. Another diffusion component is fast and surprisingly remains more or less constant with changes in temperature/viscosity. The log–log plot with the average diffusion time vs temperature-reduced viscosity yielded a similar *p*-value of 0.33 (Fig. 7a). Arrhenius's analysis with the average diffusion time also yielded similarl $E_\eta^a = 25.5 kJmol^{-1}$ as in the case of average diffusion times with 1-diffusion and anomalous fitting (E_η^a $24.7 kJmol^{-1}$, Section S11 of Supplementary Material). To the best of our knowledge, the origin of the two-time constant cannot be assigned confidently. However, the need for the second diffusion component might have arisen from the inherent heterogeneity of the system, which was reflected in the excitation wavelength dependence of the fluorescence emission in this DES. This kind of bimodal diffusion was observed in various ILs [72–74]. Patra *et al.* reported a similar kind of bimodal diffusion in methylimidazolium ILs of different chain length and comment on the presence of dynamic heterogeneity therein [72]. Hu *et al.* showed the presence of spatial heterogeneity in IL with the help of an excitation wavelength dependent emission study [75]. With the help of MD simulation Wang *et al.* proved such different domain formations in IL lead to heterogeneous environment formation, which smears out in the higher temperature range and behaves homogeneously [4]. Our data also somehow follows this kind of behaviour as with the increase in temperature the ACFs become better fitted with one diffusion than the lower temperature ACFs. In a work by Guo *et al.* with $[C_nMPy][Tf_2N]$ RTILs of varying alkyl chain length two diffusion components were observed using FCS [74]. The authors argued that mesostructure heterogeneity is responsible for this phenomenon following analogy that the translational diffusion rate of R6G differs depending upon the spatial region of the RTIL the probe molecule is experiencing [74].

Table 4
Fitting parameters of fluorescence intensity autocorrelation functions of R6G in 0.5Ac/0.3Ur/0.2Sor DES at different temperatures with two component diffusion model.

Temp (K)	τ_{D1}(μs)	N_1	τ_{D2}(μs)	N_2	$\langle\tau_D\rangle$(μs)
318	500 ± 60	0.18 ± 0.02	26900 ± 1400	0.82 ± 0.02	22150 ± 1700
323	520 ± 50	0.15 ± 0.02	23500 ± 1200	0.85 ± 0.02	20050 ± 1500
328	1000 ± 90	0.07 ± 0.02	19400 ± 600	0.93 ± 0.02	18110 ± 930
333	1430 ± 120	0.14 ± 0.02	17000 ± 500	0.86 ± 0.02	14820 ± 760
338	1200 ± 30	0.14 ± 0.02	15400 ± 400	0.86 ± 0.02	13410 ± 630
343	980 ± 60	0.17 ± 0.02	13100 ± 300	0.83 ± 0.02	11040 ± 500

The significant deviation of the *p*-value from unity suggests a breakdown of hydrodynamic viscosity dependence of solute diffusion. This deviation may be attributed to dynamic heterogeneity resulting either from spatially different diffusive relaxation rates due to inhomogeneous solution structure or from accessing the nonhydrodynamic modes owing to large angular jump, hopping, etc. [76–79]. In 2018, Gan *et al.* showed that the breakdown of SE relationship in supercooled water can arise from the temperature dependency of the effective hydrodynamic radius instead of being a constant as assumed in the SE model [80]. Very recently Shao *et al.* also showed that the deviation of SE relationship in aqueous ionic solution might be appreciated by accounting the change of hydrodynamic radius of the ions [81]. However, keeping aside the reason for such viscosity decoupling, one needs to be sure if the decoupled diffusion dynamics is a characteristic feature of DES or can be invariably seen in other molecular liquids as well. In a cross-experiment previously reported by our group with DMF [41], a decoupled diffusion with a *p*-value of 0.82 was obtained. The aspherical positively charged nature of R6G dye and DMF not being a structureless continuum was suggested for such observation [41]. In the present case, the *p*-value is much lower than 0.82, which can be taken as an indication of the presence of dynamic heterogeneity in the system. Overall, this high decoupling ($p \sim 0.33$) in the case of translational motion of the dye in this medium hints that the dye molecule does not feel the medium viscosity while diffusing. This result can be extended to understand the enzyme/substrate diffusion in case of enzymatic activity inside such viscous DES media or any alternative media in general.

3.6. Comparison with similar DES

We collected results from various acetamide-based DESs because a comparison might provide additional insight. Many acetamide-based ionic DESs were studied previously, and all of them showed considerable spatial and dynamic heterogeneity [17,18,40–44] unlike 0.6Ac/0.4Ur DES [19,38]. Replacing urea with electrolytes introduces substantial heterogeneity both in terms of spatial and dynamical arrangements [17,18,40–44]. Recently, Mukherjee *et al.* studied the microscopic heterogeneity of a DES made of acetamide, urea, and PEG-300 (0.55Ac/0.36Ur/0.09PEG) [20]. The introduction of PEG-300 introduces a mild dynamic heterogeneity in the system [20]. Here, for the comparison between non-ionic acetamide-based DESs, we have taken the previously reported data and measured them, if needed, and introduced all of them in a normalized log-log plot to show the extent of deviation in terms of dynamic heterogeneity with the present system. We have measured temperature-dependent solvation dynamics of 0.55Ac/0.36Ur/0.09PEG DES, which was previously absent in the literature. The details of those temperature-dependent solvation dynamics measurements are provided in supporting information. (Section S12, S13 and S14 of the Supplementary Material) The log-log plot of average solvation times ($\langle\tau_s\rangle$) vs $\frac{\eta}{T}$ of the two acetamide based non-ionic DESs along with the presently studied system is shown in Fig. 8a. From the figure, it is clear that solvation dynamics is almost coupled with medium viscosity in 0.6Ac/0.4Ur DES (p = 0.85), but the introduction of PEG-300 (in 0.55Ac/0.36Ur/0.09PEG DES) induces a mild decoupling (p = 0.74) which become more pronounced ($p = 0.45$) in the case of addition of sorbitol (in 0.5Ac/0.3Ur/0.2Sor DES).

The extent of decoupling in the case of inherent dynamics (in GHz region) for all three DESs follows a similar trend as in solvation dynamics (Fig. 8b). In the case of 0.55Ac/0.36Ur/0.09PEG DES, the previous work reported the decoupling in dielectric relaxation using only the first component of relaxation time [20]. To keep the uniformity in the comparison, we plotted the first component of relaxation time τ_1 (using the 2-Debye model) instead of $\langle\tau_{DR}\rangle$ in Fig. 8b. However, in our case, the *p*-value obtained for $\langle\tau_{DR}\rangle$ or τ_1 are exactly the same. For a

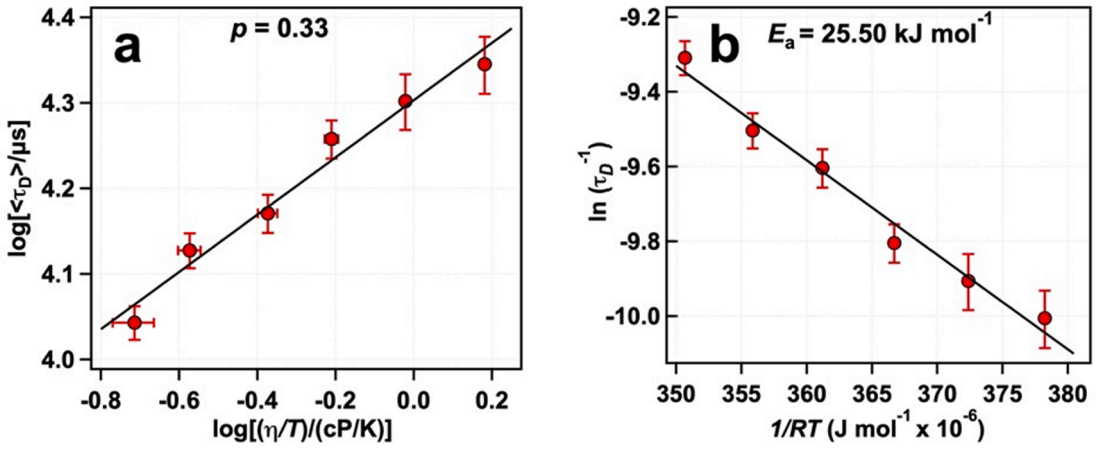

Fig. 7. (a) Log-log plot of average translational diffusion time (τ_D) vs temperature-reduced viscosity (η/T) with the linear fit represented by a solid black line. (b) Arrhenius plot of average probe diffusion time.

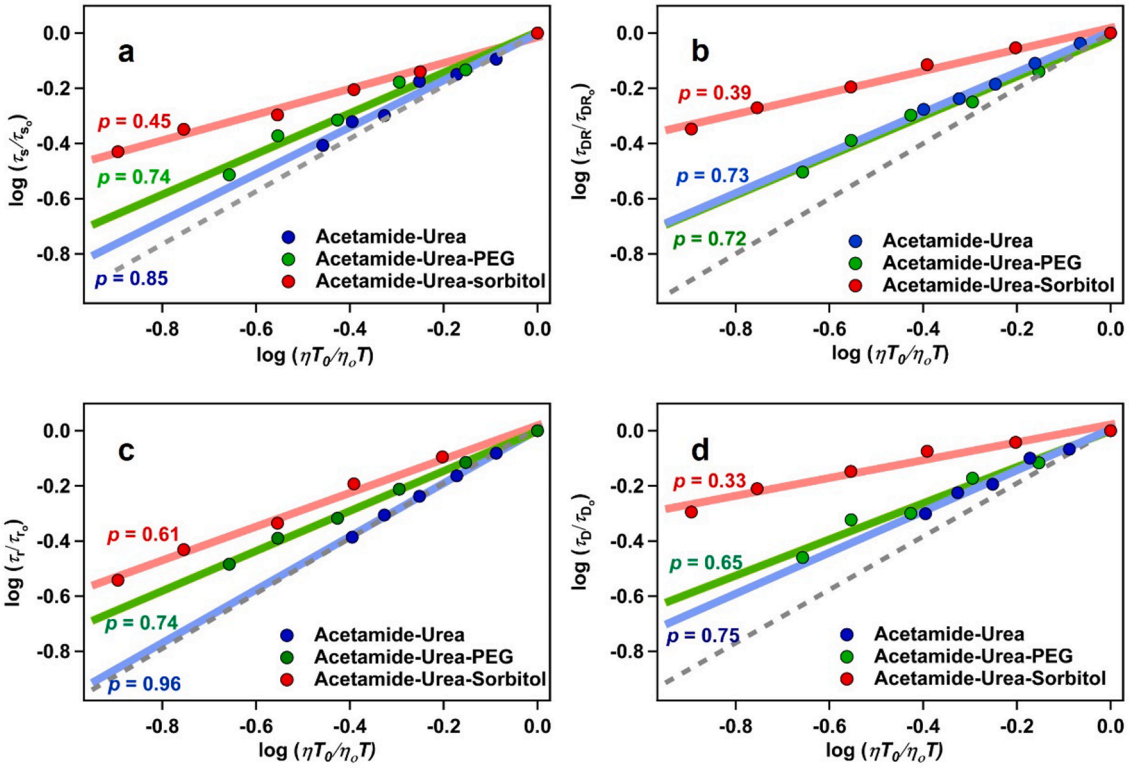

Fig. 8. Log-log plots of normalized (a) average solvation time, (b) average DR time, (c) average rotational time, and (d) average diffusion time, with temperature-reduced normalized viscosity. Here normalization has been done by taking the lowest experimental temperature; average time and viscosities at that respective lowest investigated temperature. Grey broken lines indicate the dynamics guided by the Stokes-Einstein equation(i.e. p = 1).

better understanding of the relative heterogeneity aspects in these three DESs, we fitted all the DR data (DR parameters of 0.6Ac/0.4Ur and 0.55Ac/0.36Ur/0.09PEG DES taken from literature for reconstructing ε' and ε'') with a stretched exponential function (Cole-Cole function). All the Cole-Cole fitting of our system's dielectric spectra and fitting parameters can be found in the supporting information (Section S15 and S16 of Supplementary Material). The Cole-Cole parameter β can be interpreted as a distribution of the relaxation time and $\beta < 1$ indicates that the relaxation time has an inhomogeneous distribution. In section S17 of the Supplementary Material, we have also presented temperature-dependent β for all three DESs. For a particular temperature (~333 K), β is highest for 0.6Ac/0.4Ur and decreases with the addition of PEG and sorbitol in that order.

The heterogeneity in terms of rotational dynamics for 0.55Ac/0.36Ur/0.09PEG DES is characterized by $p = 0.74$, which is substantially lower compared to the 0.6Ac/0.4Ur DES ($p = 0.96$, Fig. 8c). In the case of 0.5Ac/0.3Ur/0.2Sor DES we estimated $p = 0.61$ from fluorescence anisotropy. We measured the temperature-dependent translational dynamics of the 0.55Ac/0.36Ur/0.09PEG DES employing FCS (see sections S18 and S19 of the Supplementary Material for details). The viscosity decoupling, in this case, is pronounced compared to 0.6Ac/0.4Ur DES but less compared to the system under investigation (Fig. 8d). Taken together, one sees that introduction of a non-ionic third component to an already known DES introduces substantial microscopic heterogeneity.

To have a better insight we estimated the viscosity decoupling of the two solvation components individually (Fig. 9). Normally, the origin of the short component is believed to be from the immediate solvation shell of the probe, whereas the contribution from the extended solvation shell reflects upon a long component of the solvation dynamics. Our analysis reveals that the faster time components are severely viscosity decoupled ($p = 0.16$) suggesting that the first solvation shell remains almost intact in this DES (Fig. 9c). It might have a huge implication as to why DES, being so much viscous, can still be so efficient as a solvent media for various reactions. In the case of the other two DESs under investigation (Ac/Ur and Ac/Ur/PEG), the p-values for individual components are given in Fig. 9a and 9b. One can see that the p-value of the first component is more viscosity decoupled than the second one in all cases. However, the extent of decoupling is much less in these cases compared to Ac/Ur/Sor DES. It suggests that 0.5Ac/0.3Ur/0.2Sor DES might be a better choice as a potential reaction/biocatalytic media than the other two as the probe is experiencing much lesser viscosity than the other two DESs. Obviously, more work is needed in this regard, especially in understanding these systems in the presence of enzymes. Our future studies, taking actual enzymes, may provide further useful insights into this speculation.

Overall, an additive-induced heterogeneity is somehow prominent in this study. One very interesting but contradicting study from the Abbott group needs to be cited here where they have investigated diffusion in ethaline (0.33 choline chloride / 0.66 ethylene glycol) DES in presence of various additives [82]. They have chosen the additives as glucose, 1-pentanol, and phenol among which glucose is a room temperature solid and pentanol is a liquid and phenol is a liquid above 313 K. The interesting finding was that adding glucose increases the bulk viscosity of the system whereas the other two additives reduce it. The addition of glucose to the DES makes the choline ion (Ch^+) diffusion Stokesian type, whereas, in the case of both phenol and 1-pentanol Ch^+ diffuses in a phase that is more viscous than the bulk viscosity, indicating heterogeneities in the mixture. In the case of phenol, a change in the slope for the diffusion trend has also been observed after 313 K [82]. This finding suggests that solid additives favour the formation of a homogenous mixture, whereas liquid additives favour the formation of heterogeneous mixture. The authors assumed that the hydrogen bonding strength between the solute and the solvent (DES) has a major role to play. A similar study by Agostino *et al.* showed that when water was added to ethaline, a heterogeneous liquid was formed [83]. In the present case, both sorbitol (solid additive) and PEG-300 (liquid additive) induce a higher heterogeneity in the Ac/Ur DES, though, in the case of sorbitol, the heterogeneity is much more prominent than that of PEG-300. Although, such a conclusion cannot be conjectured from the smaller number of available studies, and more research is needed.

4. Conclusion

One important way to fine-tune DESs properties is the addition of a third component in binary DESs. The addition of sorbitol in the binary acetamide/urea DES forms a ternary 0.5Ac/0.3Ur/0.2Sor DES that has a much lower melting point [46], and is found suitable for practical application [47]. The present work demonstrates spatial and dynamic heterogeneity in 0.5Ac/0.3Ur/0.2Sor DES using steady-state, time-resolved fluorescence, dielectric relaxation, and single molecular level FCS studies.

We observed a considerable shift in the excitation wavelength-dependent emission maxima of a solvatochromic dye (C153) suggests that the system possesses considerable spatial heterogeneity. The fractional viscosity decoupling ($p \sim 0.4$) of average solvation time suggests the presence of dynamic heterogeneity in the system in the length (nm) and time (ps-ns) scale of solvation dynamics. The inherent dynamics of the medium explored using DR measurement also show a substantial decoupled dynamic ($p \sim 0.41$). The average rotational time of the probe also shows a medium viscosity decoupling ($p \sim 0.6$) suggesting a definitive but probably weaker dynamic heterogeneity in the length (nm) and time (ns) scale of anisotropy measurement. For translational dynamics, which provides information at a much larger length (μm) and timescale (μs-ms), we observed the strongest decoupling ($p \sim 0.3$) from medium viscosity suggesting a very strong dynamic heterogeneity at this higher length and time scale. Using the Arrhenius equation, we determined the activation energy of viscous flow and various dynamics that also reinforces the conclusion of strong dynamic heterogeneity of the system, which depends on the length and timescale of the measurement. The addition of PEG instead of sorbitol introduces mild dynamic heterogeneity both in translational ($p \sim 0.41$) and rotational ($p \sim 0.74$) motion, but no spatial heterogeneity. One possible reason might be the physical state of the third component (sorbitol is solid, while PEG is liquid). Future studies are necessary to understand the actual reason for the differential behaviour of these two additives, in which neutron scattering and MD simulation might help immensely. Overall, the present study might be beneficial to understand the transition of binary to ternary DESs and how the addition of a third component controls the macroscopic and microscopic properties of the DES.

Declaration of Competing Interest

The authors declare that they have no known competing financial interests or personal relationships that could have appeared to influence the work reported in this paper.

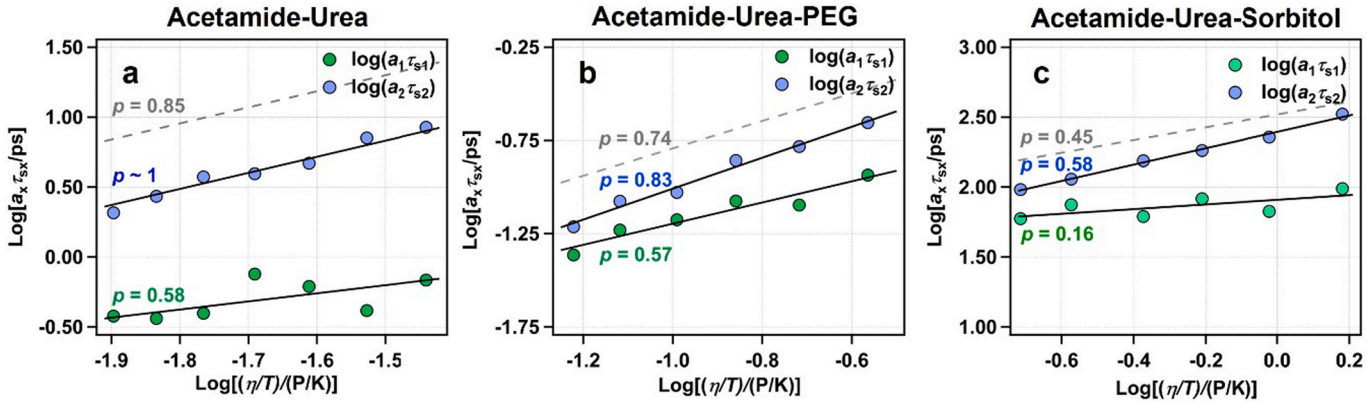

Fig. 9. Log-log plots of time components of solvation dynamics along with its contribution vs temperature reduced viscosity (η/T), with a linear fit (solid black line) for (a) 0.6Ac/0.4Ur DES, (b) 0.55Ac/0.36Ur/0.09PEG DES, and (c) 0.5Ac/0.3Ur/0.2Sor DES. The black dashed line here represents the fitting line with average solvation time and the corresponding p-value is written in the same colour.

Data availability

Data will be made available on request.

Acknowledgments

TK thanks the Prime Minister Research Fellowship, Government of India for graduate studies. ET gratefully acknowledges the Institute Post-Doctoral Fellowship (iPDF) by the Indian Institute of Technology Kanpur. ND thanks CSIR for providing graduate fellowship. Authors thank Department of Chemical Engineering, IIT Bombay, India for Karl Fischer titration. This work was supported by Japan-India Science Cooperative Program between JSPS and DST, JPJSBP120217708 (Japanese side), and DST/INT/JSPS/P-333/2021 (Indian side). PS thanks the Indian Institute of Technology Kanpur for infrastructure and support.

Appendix A. Supplementary data

Supplementary data to this article can be found online at https://doi.org/10.1016/j.molliq.2023.122882.

References

[1] K. Töpfer, A. Pasti, A. Das, S.M. Salehi, L.I. Vazquez-Salazar, D. Rohrbach, T. Feurer, P. Hamm, M. Meuwly, Structure, Organization, and Heterogeneity of Water-Containing Deep Eutectic Solvents, accessed March 20, 2023, J. Am. Chem. Soc. 144 (2022) 14170–14180, https://pubs.acs.org/doi/full/10.1021/jacs.2c04169.
[2] J.R. Krahn, T.P. Lodge, Spatial heterogeneity of solvent dynamics in multicomponent polymer solutions, J. Phys. Chem. 99 (1995) 8338–8348, https://doi.org/10.1021/j100020a069.
[3] D.F. Kienle, R.M. Falatach, J.L. Kaar, D.K. Schwartz, Correlating structural and functional heterogeneity of immobilized enzymes, ACS Nano 12 (2018) 8091–8103. https://pubs.acs.org/doi/full/10.1021/acsnano.8b02956.
[4] Y.L. Wang, B. Li, S. Sarman, F. Mocci, Z.Y. Lu, J. Yuan, A. Laaksonen, M.D. Fayer, Microstructural and Dynamical Heterogeneities in Ionic Liquids, Chem. Rev. 120 (2020) 5798–5877, https://doi.org/10.1021/acs.chemrev.9b00693.
[5] M.D. Ediger, Spatially heterogeneous dynamics in supercooled liquids, Annu. Rev. Phys. Chem. 51 (2000) 99–128, https://doi.org/10.1146/annurev.physchem.51.1.99.
[6] R. Richert, Heterogeneous dynamics in liquids: Fluctuations in space and time, J. Phys. Condens. Matter 14 (2002) R703, https://doi.org/10.1088/0953-8984/14/23/201.
[7] H. Jin, X. Li, M. Maroncelli, Heterogeneous solute dynamics in room temperature ionic liquids, J. Phys. Chem. B 111 (2007) 13473–13478, https://doi.org/10.1021/jp077226.
[8] T. Hoshino, S. Fujinami, T. Nakatani, Y. Kohmura, Dynamical Heterogeneity near Glass Transition Temperature under Shear Conditions, Phys. Rev. Lett. 124 (2020), 118004, https://doi.org/10.1103/PhysRevLett.124.118004.
[9] H. Sillescu, Heterogeneity at the glass transition: A review, J. Non Cryst. Solids 243 (1999) 81–108, https://doi.org/10.1016/S0022-3093(98)00831-X.
[10] L.A. Deschenes, D.A. Vanden Bout, Single-molecule studies of heterogeneous dynamics in polymer melts near the glass transition, Science 292 (2001) (1979) 255–258, https://doi.org/10.1126/science.1056430.
[11] P. Kumar, S.V. Buldyrev, S.R. Becker, P.H. Poole, F.W. Starr, H.E. Stanley, Relation between the Widom line and the breakdown of the Stokes-Einstein relation in supercooled water, PNAS 104 (2007) 9575–9579, https://doi.org/10.1073/pnas.0702608104.
[12] L. Berthier, G. Biroli, J.P. Bouchaud, L. Cipelletti, D. El Masri, D. L'Hôte, F. Ladieu, M. Pierno, Direct experimental evidence of a growing length scale accompanying the glass transition, Science 310 (2005) (1979) 1797–1800, https://doi.org/10.1126/science.1120714.
[13] D. Kivelson, S.A. Kivelson, X. Zhao, Z. Nussinov, G. Tarjus, A thermodynamic theory of supercooled liquids, Physica A 219 (1995) 27–38, https://doi.org/10.1016/0378-4371(95)00140-3.
[14] S.H. Chen, F. Mallamace, C.Y. Mou, M. Broccio, C. Corsaro, A. Faraone, L. Liu, The violation of the Stokes-Einstein relation in supercooled water, PNAS 103 (2006) 12974–12978, https://doi.org/10.1073/pnas.0603253103.
[15] N. Das, P. Sen, Dynamic heterogeneity and viscosity decoupling: Origin and analytical prediction, PCCP 23 (2021) 15749–15757, https://doi.org/10.1039/d1cp01804c.
[16] M.L. Horng, J.A. Gardecki, M. Maroncelli, Rotational dynamics of coumarin 153: Time-dependent friction, dielectric friction, and other nonhydrodynamic effects, Chem. A Eur. J. 101 (1997) 1030–1047, https://doi.org/10.1021/jp962921v.
[17] B. Guchhait, S. Das, S. Daschakraborty, R. Biswas, Interaction and dynamics of (alkylamide + electrolyte) deep eutectics: Dependence on alkyl chain-length, temperature, and anion identity, J. Chem. Phys. 140 (2014), 104514, https://doi.org/10.1063/1.4866178.
[18] B. Guchhait, S. Daschakraborty, R. Biswas, Medium decoupling of dynamics at temperatures ~100 K above glass-transition temperature: A case study with (acetamide + lithium bromidenitrate) melts, J. Chem. Phys. 136 (2012), 174503, https://doi.org/10.1063/1.4705315.
[19] A. Das, S. Das, R. Biswas, Density relaxation and particle motion characteristics in a non-ionic deep eutectic solvent (acetamide + urea): Time-resolved fluorescence measurements and all-atom molecular dynamics simulations, J. Chem. Phys. 142 (2015), 034505, https://doi.org/10.1063/1.4906119.
[20] K. Mukherjee, E. Tarif, A. Barman, R. Biswas, Dynamics of a PEG based non-ionic deep eutectic solvent: Temperature dependence, Fluid Phase Equilib. 448 (2017) 22–29, https://doi.org/10.1016/j.fluid.2017.05.003.
[21] S.S. Hossain, S. Paul, A. Samanta, Liquid Structure and Dynamics of Tetraalkylammonium Bromide-Based Deep Eutectic Solvents: Effect of Cation Chain Length, J. Phys. Chem. B 123 (2019) 6842–6850, https://doi.org/10.1021/acs.jpcb.9b04955.
[22] S.S. Hossain, A. Samanta, How do the hydrocarbon chain length and hydroxyl group position influence the solute dynamics in alcohol-based deep eutectic solvents? PCCP 20 (2018) 24613–24622, https://doi.org/10.1039/c8cp04859b.
[23] A. Mahapatra, M. Chakraborty, S. Barik, M. Sarkar, Comparison between pyrrolidinium-based and imidazolium-based dicationic ionic liquids: Intermolecular interaction, structural organization, and solute dynamics, PCCP 23 (2021) 21029–21041, https://doi.org/10.1039/d1cp02790e.
[24] S. Barik, M. Chakraborty, M. Sarkar, How Does Addition of Lithium Salt Influence the Structure and Dynamics of Choline Chloride-Based Deep Eutectic Solvents? J. Phys. Chem. B 124 (2020) 2864–2878, https://doi.org/10.1021/acs.jpcb.9b11947.
[25] S.S. Hossain, A. Samanta, Solute rotation and solvation dynamics in deep eutectic solvents, Chemical Physics Impact. 3 (2021), 100043, https://doi.org/10.1016/j.chphi.2021.100043.
[26] E.L. Smith, A.P. Abbott, K.S. Ryder, Deep Eutectic Solvents (DESs) and Their Applications, Chem. Rev. 114 (2014) 11060–11082, https://doi.org/10.1021/cr300162p.
[27] B.B. Hansen, S. Spittle, B. Chen, D. Poe, Y. Zhang, J.M. Klein, A. Horton, L. Adhikari, T. Zelovich, B.W. Doherty, B. Gurkan, E.J. Maginn, A. Ragauskas, M. Dadmun, T.A. Zawodzinski, G.A. Baker, M.E. Tuckerman, R.F. Savinell, J. R. Sangoro, Deep Eutectic Solvents: A Review of Fundamentals and Applications, Chem. Rev. 121 (2021) 1232–1285, https://doi.org/10.1021/acs.chemrev.0c00385.
[28] C. Florindo, F. Lima, B.D. Ribeiro, I.M. Marrucho, Deep eutectic solvents: overcoming 21st century challenges, Curr Opin Green Sustain Chem. 18 (2019) 31–36, https://doi.org/10.1016/j.cogsc.2018.12.003.
[29] A. Paiva, R. Craveiro, I. Aroso, M. Martins, R.L. Reis, A.R.C. Duarte, Natural deep eutectic solvents - Solvents for the 21st century, ACS Sustain. Chem. Eng. 2 (2014) 1063–1071, https://doi.org/10.1021/sc500096j.
[30] F.M. Perna, P. Vitale, V. Capriati, Deep eutectic solvents and their applications as green solvents, Curr Opin Green Sustain Chem. 21 (2020) 27–33, https://doi.org/10.1016/j.cogsc.2019.09.004.
[31] M. Jablonský, A. Škulcová, J. Šima, Use of deep eutectic solvents in polymer chemistry–a review, Molecules 24 (2019) 3978, https://doi.org/10.3390/molecules24213978.
[32] C. Padwal, H.D. Pham, S. Jadhav, T.T. Do, J. Nerkar, L.T.M. Hoang, A. Kumar Nanjundan, S.G. Mundree, D.P. Dubal, Deep Eutectic Solvents: Green Approach for Cathode Recycling of Li-Ion Batteries, Adv. Energy Sustain. Res. 3 (2022) 2100133, https://doi.org/10.1002/aesr.202100133.
[33] N. Yadav, P. Venkatesu, Current understanding and insights towards protein stabilization and activation in deep eutectic solvents as sustainable solvent media, PCCP 24 (2022) 13474–13509, https://doi.org/10.1039/D2CP00084A.
[34] S.C. Cunha, J.O. Fernandes, Extraction techniques with deep eutectic solvents, TrAC -, Trends Anal. Chem. 105 (2018) 225–239, https://doi.org/10.1016/j.trac.2018.05.001.
[35] P. Liu, J.W. Hao, L.P. Mo, Z.H. Zhang, Recent advances in the application of deep eutectic solvents as sustainable media as well as catalysts in organic reactions, RSC Adv. 5 (2015) 48675–48704, https://doi.org/10.1039/C5RA05746A.
[36] D.O. Abranches, M.A.R. Martins, L.P. Silva, N. Schaeffer, S.P. Pinho, J.A. P. Coutinho, Phenolic hydrogen bond donors in the formation of non-ionic deep eutectic solvents: The quest for type v des, Chem. Commun. 55 (2019) 10253–10256, https://doi.org/10.1039/c9cc04846d.
[37] N. Subba, N. Das, P. Sen, Partial Viscosity Decoupling of Solute Solvation, Rotation, and Translation Dynamics in Lauric Acid/Menthol Deep Eutectic Solvent: Modulation of Dynamic Heterogeneity with Length Scale, J. Phys. Chem. B 124 (2020) 6875–6884, https://doi.org/10.1021/acs.jpcb.0c04379.
[38] N. Subba, K. Polok, P. Piatkowski, B. Ratajska-Gadomska, R. Biswas, W. Gadomski, P. Sen, Temperature-Dependent Ultrafast Solvation Response and Solute Diffusion in Acetamide-Urea Deep Eutectic Solvent, J. Phys. Chem. B 123 (2019) 9212–9221, https://doi.org/10.1021/ACS.JPCB.9B07794.
[39] Y. Cui, J.C. Rushing, S. Seifert, N.M. Bedford, D.G. Kuroda, Molecularly Heterogeneous Structure of a Nonionic Deep Eutectic Solvent Composed of N-Methylacetamide and Lauric Acid, J. Phys. Chem. B 123 (2019) 3984–3993, https://doi.org/10.1021/acs.jpcb.8b11732.
[40] K. Mukherjee, S. Das, J. Rajbangshi, E. Tarif, A. Barman, R. Biswas, Temperature-Dependent Dielectric Relaxation in Ionic Acetamide Deep Eutectics: Partial Viscosity Decoupling and Explanations from the Simulated Single-Particle Reorientation Dynamics and Hydrogen-Bond Fluctuations, J. Phys. Chem. B 125 (2021) 12552–12567, https://doi.org/10.1021/acs.jpcb.1c07299.
[41] N. Subba, E. Tarif, P. Sen, R. Biswas, Subpicosecond Solvation Response and Partial Viscosity Decoupling of Solute Diffusion in Ionic Acetamide Deep Eutectic

Solvents: Fluorescence Up-Conversion and Fluorescence Correlation Spectroscopic Measurements, J. Phys. Chem. B 124 (2020) 1995–2005, https://doi.org/10.1021/acs.jpcb.0c00061.
[42] K. Mukherjee, A. Das, S. Choudhury, A. Barman, R. Biswas, Dielectric Relaxations of (Acetamide + Electrolyte) Deep Eutectic Solvents in the Frequency Window, 0.2 ≤ ν/GHz ≤ 50: Anion and Cation Dependence, J. Phys. Chem. B 119 (2015) 8063–8071, https://doi.org/10.1021/acs.jpcb.5b01502.
[43] H.A.R. Gazi, B. Guchhait, S. Daschakraborty, R. Biswas, Fluorescence dynamics in supercooled (acetamide + calcium nitrate) molten mixtures, Chem. Phys. Lett. 501 (2011) 358–363, https://doi.org/10.1016/j.cplett.2010.12.003.
[44] B. Guchhait, H. Al Rasid Gazi, H.K. Kashyap, R. Biswas, Fluorescence spectroscopic studies of (acetamide + sodium/potassium thiocyanates) molten mixtures: Composition and temperature dependence, J. Phys. Chem. B. 114 (2010) 5066–5081. 10.1021/jp1001176.
[45] K. Mukherjee, S. Das, E. Tarif, A. Barman, R. Biswas, Dielectric relaxation in acetamide + urea deep eutectics and neat molten urea: Origin of time scales via temperature dependent measurements and computer simulations, J. Chem. Phys. 149 (2018), 124501, https://doi.org/10.1063/1.5040071.
[46] N. Subba, P. Sahu, N. Das, P. Sen, Rational design, preparation and characterization of a ternary non-ionic room-temperature deep eutectic solvent derived from urea, acetamide, and sorbitol, J. Chem. Sci. 133 (2021) 25, https://doi.org/10.1007/s12039-020-01866-2.
[47] N. Das, T. Khan, N. Subba, P. Sen, Correlating Bromelain's activity with its structure and active-site dynamics and the medium's physical properties in a hydrated deep eutectic solvent, PCCP 23 (2021) 9337–9346, https://doi.org/10.1039/d1cp00046b.
[48] B. Sengupta, A. Acharyya, P. Sen, Elucidation of the local dynamics of domain-III of human serum albumin over the ps–μs time regime using a new fluorescent label, PCCP 18 (2016) 28548–28555, https://doi.org/10.1039/C6CP05743H.
[49] A. Das, G. Sharma, N. Kamatham, R. Prabhakar, P. Sen, V. Ramamurthy, Ultrafast Solvation Dynamics Reveal that Octa Acid Capsule's Interior Dryness Depends on the Guest, Chem. A Eur. J. 123 (2019) 5928–5936, https://doi.org/10.1021/acs.jpca.9b04626.
[50] M. Maroncelli, G.R. Fleming, Picosecond solvation dynamics of coumarin 153: The importance of molecular aspects of solvation, J. Chem. Phys. 86 (1987) 6221–6239, https://doi.org/10.1063/1.452460.
[51] J.R. Lakowicz, Principles of fluorescence spectroscopy, Springer, 2006, doi: 10.1007/978-0-387-46312-4.
[52] M.L. Horng, J.A. Gardecki, A. Papazyan, M. Maroncelli, Subpicosecond measurements of polar solvation dynamics: Coumarin 153 revisited, J. Phys. Chem. 99 (1995) 17311–17337, https://doi.org/10.1021/J100048A004.
[53] N. Yamamoto, K. Ohta, A. Tamura, K. Tominaga, Broadband Dielectric Spectroscopy on Lysozyme in the Sub-Gigahertz to Terahertz Frequency Regions: Effects of Hydration and Thermal Excitation, accessed March 20, 2023, J. Phys. Chem. B 120 (2016) 4743–4755, https://pubs.acs.org/doi/full/10.1021/acs.jpcb.6b01491.
[54] Y. Kadomura, N. Yamamoto, K. Tominaga, Broadband dielectric spectroscopy from sub GHz to THz of hydrated lipid bilayer of DMPC, Eur. Phys. J. E 42 (139) (2019) 1–8, https://doi.org/10.1140/EPJE/I2019-11901-1.
[55] N. Das, P. Sen, Structural, Functional, and Dynamical Responses of a Protein in a Restricted Environment Imposed by Macromolecular Crowding, Biochemistry 57 (2018) 6078–6089, https://doi.org/10.1021/acs.biochem.8b00599.
[56] N. Das, P. Sen, Shape-Dependent Macromolecular Crowding on the Thermodynamics and Microsecond Conformational Dynamics of Protein Unfolding Revealed at the Single-Molecule Level, J. Phys. Chem. B 124 (2020) 5858–5871, https://doi.org/10.1021/acs.jpcb.0c03897.
[57] N. Das, P. Sen, Macromolecular crowding: how shape and interaction affect the structure, function, conformational dynamics and relative domain movement of a multi-domain protein, PCCP 24 (2022) 14242–14256, https://doi.org/10.1039/D1CP04842B.
[58] T. Wohland, S. Maiti, R. Macháň, An Introduction to Fluorescence Correlation Spectroscopy, IOP Publishing, 2020, doi: 10.1088/978-0-7503-2080-1.
[59] C.B. Müller, A. Loman, V. Pacheco, F. Koberling, D. Willbold, W. Richtering, J. Enderlein, Precise measurement of diffusion by multi-color dual-focus fluorescence correlation spectroscopy, EPL 83 (2008) 46001, https://doi.org/10.1209/0295-5075/83/46001.
[60] J. Hunger, A. Stoppa, S. Schrödle, G. Hefter, R. Buchner, Temperature dependence of the dielectric properties and dynamics of ionic liquids, ChemPhysChem 10 (2009) 723–733, https://doi.org/10.1002/cphc.200800483.
[61] M. Petrowsky, R. Freeh, Application of the compensated arrhenius formalism to dielectric relaxation, J. Phys. Chem. B 113 (2009) 16118–16123, https://doi.org/10.1021/jp907018s.
[62] A.P. Demchenko, The red-edge effects: 30 years of exploration, Luminescence 17 (2002) 19–42, https://doi.org/10.1002/bio.671.
[63] N. Das, S. Sahu, T. Khan, P. Sen, Site-specific Heterogeneity of Multi-domain Human Serum Albumin and its Origin: A Red Edge Excitation Shift Study, Photochem. Photobiol. 99 (2023) 538–546.
[64] A. Das, R. Biswas, Dynamic Solvent Control of a Reaction in Ionic Deep Eutectic Solvents: Time-Resolved Fluorescence Measurements of Reactive and Nonreactive Dynamics in (Choline Chloride + Urea) Melts, J. Phys. Chem. B 119 (2015) 10102–11013, https://doi.org/10.1021/acs.jpcb.5b04936.
[65] E. Tarif, J. Mondal, R. Biswas, How frictional response during solute solvation controls solute rotation in naturally abundant deep eutectic solvent (NADES)? A case study with amino acid derivative containing DES, J. Mol. Liq. 303 (2020), 112451, https://doi.org/10.1016/j.molliq.2020.112451.
[66] T. Azumi, K.I. Itoh, H. Shiraishi, Shift of emission band upon the excitation at the long wavelength absorption edge. III. Temperature dependence of the shift and correlation with the time dependent spectral shift, J. Chem. Phys. 65 (1976) 2550–2555, https://doi.org/10.1063/1.433440.
[67] K.I. Itoh, T. Azumi, Shift of the emission band upon excitation at the long wavelength absorption edge. II. Importance of the solute-solvent interaction and the solvent reorientation relaxation process, J. Chem. Phys. 62 (1975) 3431–3438, https://doi.org/10.1063/1.430977.
[68] R.S. Fee, M. Maroncelli, Estimating the time-zero spectrum in time-resolved emmsion measurements of solvation dynamics, Chem. Phys. 183 (1994) 235–247, https://doi.org/10.1016/0301-0104(94)00019-0.
[69] E. Tarif, J. Mondal, R. Biswas, Interaction and Dynamics in a Fully Biodegradable Glucose-Containing Naturally Abundant Deep Eutectic Solvent: Temperature-Dependent Time-Resolved Fluorescence Measurements, J. Phys. Chem. B 123 (2019) 9378–9387, https://doi.org/10.1021/acs.jpcb.9b06783.
[70] H. Jin, G.A. Baker, S. Arzhantsev, J. Dong, M. Maroncelli, Solvation and rotational dynamics of coumarin 153 in ionic liquids: Comparisons to conventional solvents, J. Phys. Chem. B 111 (2007) 7291–7302, https://doi.org/10.1021/jp070923h.
[71] P. Schwille, J. Korlach, W.W. Webb, Fluorescence correlation spectroscopy with single-molecule sensitivity on cell and model membranes, Cytometry 36 (1999) 176–182.
[72] S. Patra, A. Samanta, Microheterogeneity of some imidazolium ionic liquids as revealed by fluorescence correlation spectroscopy and lifetime studies, J. Phys. Chem. B 116 (2012) 12275–12283, https://doi.org/10.1021/jp3061202.
[73] E.C. Wu, H.J. Kim, L.A. Peteanu, Spectroscopic and MD Study of Dynamic and Structural Heterogeneities in Ionic Liquids, J. Phys. Chem. B 121 (2017) 100–1107, https://doi.org/10.1021/acs.jpcb.6b10678.
[74] J. Guo, G.A. Baker, P.C. Hillesheim, S. Dai, R.W. Shaw, S.M. Mahurin, Fluorescence correlation spectroscopy evidence for structural heterogeneity in ionic liquids, PCCP 13 (2011) 12395–12398, https://doi.org/10.1039/c1cp20929a.
[75] Z. Hu, C.J. Margulis, Heterogeneity in a room-temperature ionic liquid: Persistent local environments and the red-edge effect, Proc. Natl. Acad. Sci. 103 (2006) 831–836, https://doi.org/10.1073/pnas.0507364103.
[76] S. Dueby, S. Daschakraborty, Size dependence of solute's translational jump-diffusion in solvent: Relationship between trapping and jump-diffusion, Chem. Phys. Lett. 806 (2022), 140059.
[77] S.R. Becker, P.H. Poole, F.W. Starr, Fractional Stokes-Einstein and Debye-Stokes-Einstein relations in a network-forming liquid, accessed March 20, 2023, Phys. Rev. Lett. 97 (2006), 055901, https://journals.aps.org/prl/abstract/10.1103/PhysRevLett.97.055901.
[78] S. Daschakraborty, V. Dubey, Breakdown of the Stokes−Einstein relation in supercooled water/ methanol binary mixtures: Explanation using the translational jump-diffusion approach, accessed March 20, 2023, J. Phys. Chem. B 124 (2020) 10398–10408, https://pubs.acs.org/doi/full/10.1021/acs.jpcb.0c07318.
[79] L. Xu, F. Mallamace, Z. Yan, F.W. Starr, S. V. Buldyrev, H. Eugene Stanley, Appearance of a fractional Stokes–Einstein relation in water and a structural interpretation of its onset, Nature Physics 2009 5:8. 5 (2009) 565–569. 10.1038/nphys1328.
[80] G. Ren, L. Chen, Y. Wang, Dynamic heterogeneity in aqueous ionic solutions, PCCP 20 (2018) 21313–21324, https://doi.org/10.1039/c8cp02787k.
[81] Y. Shao, M. Hellström, A. Yllö, J. Mindemark, K. Hermansson, J. Behler, C. Zhang, Temperature effects on the ionic conductivity in concentrated alkaline electrolyte solutions, PCCP 22 (2020) 10426–10430, https://doi.org/10.1039/c9cp06479f.
[82] R. Häkkinen, O. Alshammari, V. Timmermann, C. D'Agostino, A. Abbott, Nanoscale Clustering of Alcoholic Solutes in Deep Eutectic Solvents Studied by Nuclear Magnetic Resonance and Dynamic Light Scattering, ACS Sustain. Chem. Eng. 7 (2019) 15086–15092, https://doi.org/10.1021/acssuschemeng.9b03771.
[83] C. D'Agostino, L.F. Gladden, M.D. Mantle, A.P. Abbott, E.I. Ahmed, A.Y.M. Al-Murshedi, R.C. Harris, Molecular and ionic diffusion in aqueous-deep eutectic solvent mixtures: Probing inter-molecular interactions using PFG NMR, PCCP 17 (2015) 15297–15304, https://doi.org/10.1039/c5cp01493j.

Supporting Information

Multiple Evidences for Molecular Level Heterogeneity in a Non-ionic Biocatalytic Deep Eutectic Solvent

Tanmoy Khan,[#,1] Ejaj Tarif,[#,1] Yuto Awano,[2] Lou Serafin Lozada,[2] Nilimesh Das,[1] Keisuke Tominaga[2,3] and Pratik Sen[1,*]

[1]Department of Chemistry, Indian Institute of Technology Kanpur, Kanpur – 208 016, UP, India

[2]Department of Chemistry, Graduate School for Science, Kobe University, Nada, Kobe 657-8501 Japan.

[3]Molecular Photoscience Rersearch Center, Kobe University, Nada, Kobe 657-8501 Japan.

CONTENTS

Section S1: Dielectric Relaxation Measurement

The operating frequency window of the instrument is $0.5 \leq \nu/\mathrm{GHz} \leq 20$. Approximately 25 mL of DES was used for measurements in each case. Obtained frequency (ν) dependent complex relative permittivity, $\varepsilon^*(\nu)$, is expressed as follows

$$\varepsilon^*(\nu) = \varepsilon'(\nu) - i\varepsilon''(\nu), \quad (1)$$

where $\varepsilon'(\nu)$ and $\varepsilon''(\nu)$ represent real and imaginary parts of the complex permittivity ($\varepsilon^*(\nu)$), respectively. The temperature-dependent measured ε*(ν) for DESs were then fitted by a sum of the Havriliak−Negami (HN) equation

$$\varepsilon^*(\nu) = \varepsilon_\infty + \sum_{j=1}^{n} \frac{\Delta\varepsilon_j}{\left[1+(i2\pi\nu\tau_j)^{\beta_j}\right]^{\alpha_j}} \quad (2)$$

$\varepsilon_\infty = \varepsilon(\nu \to \infty)$ is the permittivity at infinite frequency, $\Delta\varepsilon$, τ, α, and β represent the dielectric relaxation amplitude, relaxation time, Cole−Davidson and Cole−Cole parameters, respectively. Note that $\alpha = 1$, $\beta = 1$ describes relaxation via the Debye model, and for $\alpha = 1$, $0 < \beta < 1$, the expression becomes Cole−Cole function whereas $\beta = 1$, $0 < \alpha < 1$, indicate Cole−Davidson relation. The Cole−Cole parameter β can be interpreted distribution of the relaxation time and $\beta < 1$ also tells the relaxation time has an inhomogeneous distribution. In this study, the obtained DRS data of 0.5Ac/0.3Ur/0.2Sor are best fitted with a multi-Debye fitting function.

Section S2: FCS measurement

FCS measurements were performed using an instrument built in our laboratory. An inverted microscope (IX-71, Olympus, Japan) was used for this setup coupled with a 532 nm CW laser (MGL-III-532-5 mW, CNI, China) excitation source. A 60X water immersion objective lens with a 1.2 numerical aperture was used to focus the excitation light into the sample at a distance of ~ 40 μm from the surface of the coverslip. The emitted photons were collected using the same objective lens and were focused on a multimode fibre patch cord of 50 μm diameter after passing through a dichroic (ZT532rdc, Chroma Tech. Corp.) and an emission filter (605/70m, Chroma Tech. Corp.). The fluorescence signal was then directed toward a photon counting module (SPCM-AQRH-13-FC, Excelitas) and then to a correlator card (FLEX990EM-12D, Correlator.com, USA) to generate an autocorrelation function, $G(\tau)$. For a temperature-dependent experiment, we used a temperature cell designed in our laboratory.[1] Its bottom is attached to the coverslip, over which the sample is kept for measurement. The temperature of the cell was controlled using a temperature-controlled water circulation system (LLCB-202, Labocon, UK). The autocorrelation function, $G(\tau)$, as generated from the temporal fluctuation of the fluorescence intensity using the correlator card can be described as[2, 3]

$$G(\tau) = \frac{\langle \delta F(t) \delta F(t+\tau) \rangle}{\langle F(t) \rangle^2} \qquad (3)$$

Here, $\langle F(t) \rangle$ is the average fluorescence intensity; $\delta F(t)$ and $\delta F(t + \tau)$ are the quantity of fluctuation in intensity around the mean value at time t and $(t + \tau)$, respectively. Autocorrelation function for different models has been described in the materials and method section of the main manuscript.

Section S3: Temperature Dependent Absorption and Emission of C153 in 0.5Ac/0.3Ur/0.2Sor DES

Table S1: Temperature dependent absorption and emission maxima of coumarin 153 in 0.5Ac/0.3Ur/0.2Sor DES.

Temperature (K)	**Absorption Maximum (nm)**	**Absorption Maximum (cm^{-1})**	**Emission maximum (nm)**	**Emission maximum (cm^{-1})**
298	433.7	23057.4	534.5	18709.1
303	433.2	23084.0	536.6	18635.8
308	433.0	23094.7	538.4	18573.5
313	433.0	23094.7	539.8	18525.4
318	432.7	23110.7	541.2	18477.4
323	432.5	23121.4	542.0	18450.2
328	432.3	23132.1	542.7	18426.4
333	432.2	23137.4	543.1	18412.8
338	432.0	23148.1	543.6	18395.9
343	431.9	23153.5	544.0	18382.4

Section S4: Excitation wavelength dependent emission of C153 in 0.5Ac/0.3Ur/0.2Sor DES

Table S2: Excitation dependent emission maxima of coumarin 153 in 0.5Ac/0.3Ur/0.2Sor DES.

λ_{ex} (nm)	λ_{em}^{max} (nm)	$\bar{\nu}_{em}^{max}$ (cm^{-1})
375	532.4	18782.9
385	532.4	18782.9
395	532.8	18768.8
405	533.1	18758.2
415	533.6	18740.6
425	533.9	18730.1
435	534.5	18709.1
445	534.6	18705.6
455	534.9	18695.1
465	535.0	18691.6
475	535.9	18660.2
485	537.0	18622.0
495	537.3	18611.6
505	539.8	18525.4
515	542.4	18436.6

Section S5: Temperature dependent fluorescence transients of C153 in 0.5Ac/0.3Ur/0.2Sor DES

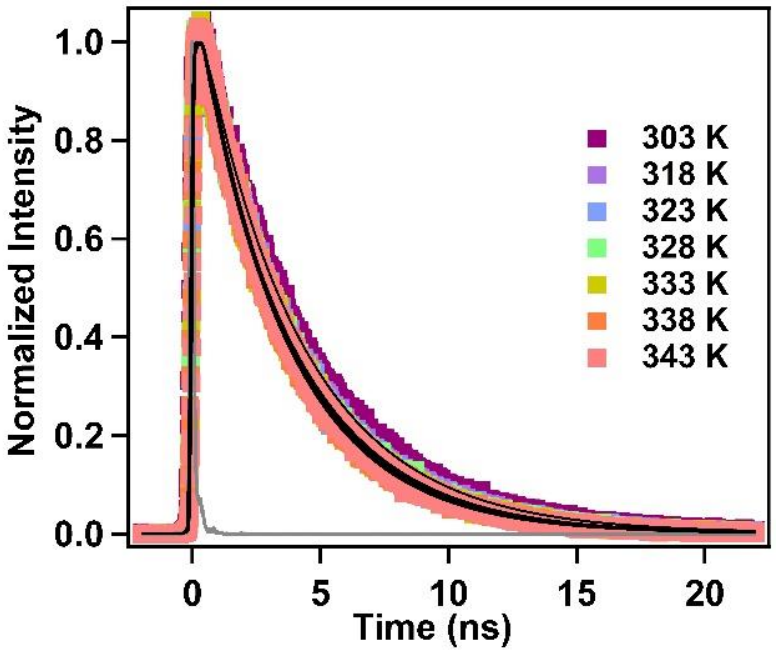

Figure S1: Temperature-dependent lifetime of coumarin 153 in Ac-Ur-Sor DES

Section S6: Temperature dependent average fluorescence lifetime C153 in 0.5Ac/0.3Ur/0.2Sor DES

Table S3: Biexponential fitting parameters of Temperature dependent lifetime of coumarin 153 in Ac-Ur-Sor DES**.**

Temp (K)	A_1 (%)	τ_1 (ns)	A_2 (%)	τ_2 (ns)	τ_{avg} (ns)
303	4.0	0.34	96.0	4.02	3.87
318	13.0	0.44	87.0	3.79	3.35
323	11.0	0.33	89.0	3.69	3.32
328	14.0	0.26	86.0	3.65	3.17
333	13.0	0.26	87.0	3.58	3.15
338	11.6	0.33	88.4	3.54	3.17
343	10.1	0.22	89.9	3.51	3.17

Section S7: Representative raw data for solvation dynamics of C153 in 0.5Ac/0.3Ur/0.2Sor DES

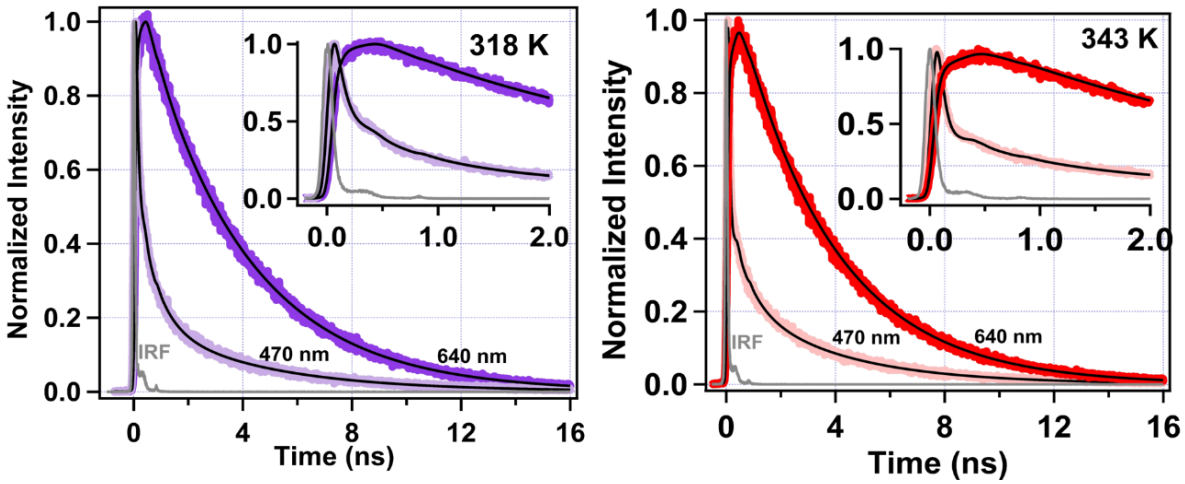

Figure S2: Fluorescence transients of the blue and red edge of steady-state emission of C153 in 0.5Ac/0.3Ur/0.2Sor DES at two extreme experimental temperatures.

Section S8: Raw data of Dielectric measurement of 0.5Ac/0.3Ur/0.2Sor DES with 2-Debye fitting

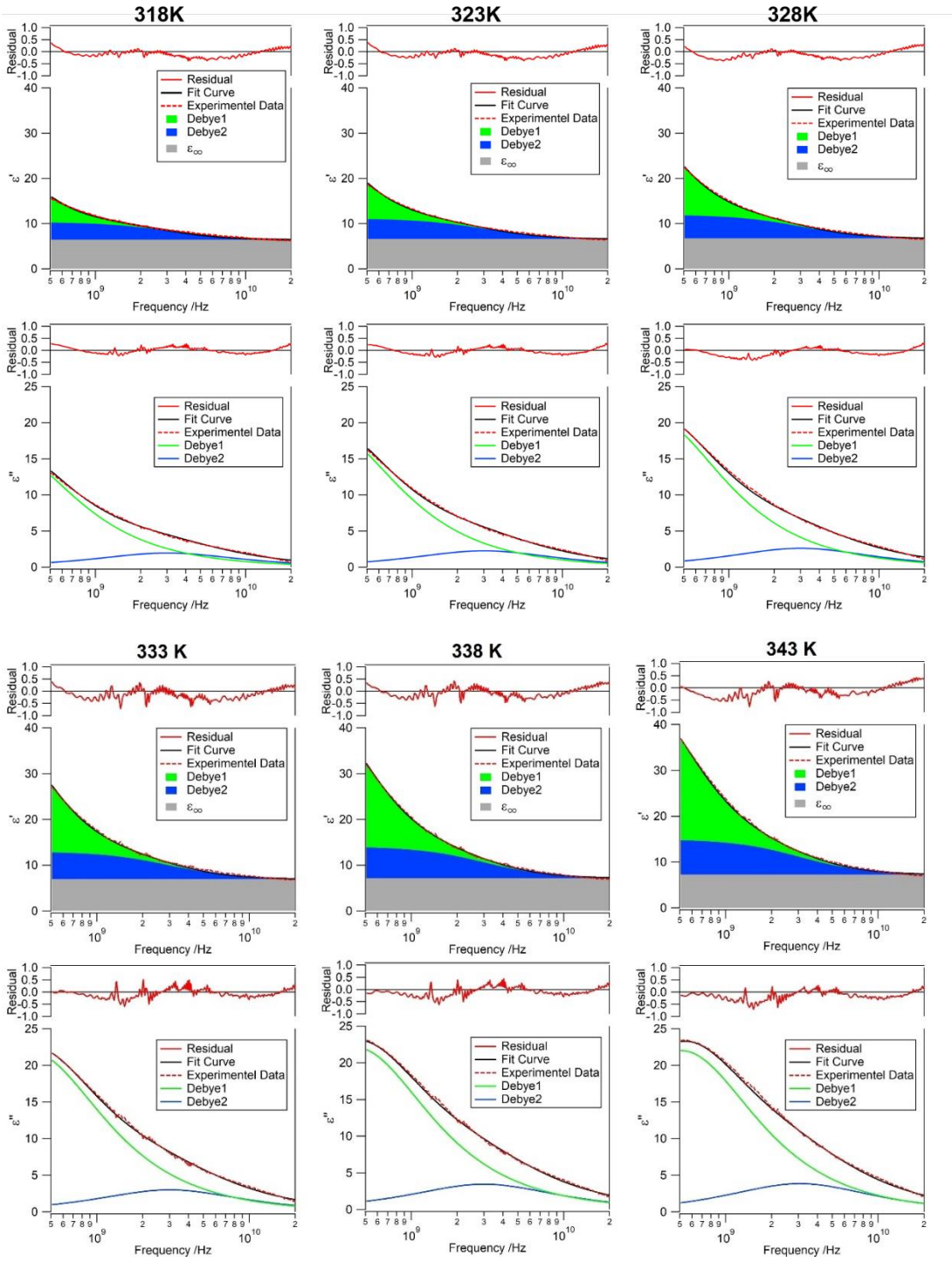

Figure S3: Fitting of real (ε') and imaginary (ε'') part of the complex dielectric spectra of 0.5Ac/0.3Ur/0.2Sor DES at different temperatures with the 2-Debye fit (equation 2 when $\alpha = 1$, $\beta = 1$ and n = 2). The upper panel for each temperature represent the real part whereas the lower is the imaginary part.

Section S9: Representative raw data for Rotational dynamics of C153 in 0.5Ac/0.3Ur/0.2Sor DES

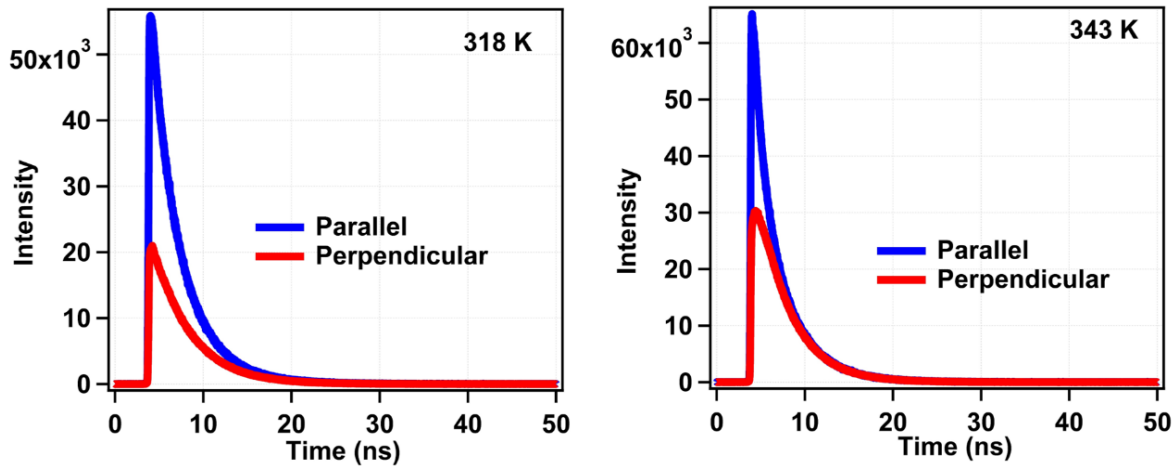

Figure S4: Raw data for fluorescence anisotropy at two extreme experimental temperature

Section S10: Fitting parameter of fluorescence intensity autocorrelation function with 1-D and anomalous fitting function of R6G in 0.5Ac/0.3Ur/0.2Sor DES

Table S4: Fitting parameter of fluorescence intensity autocorrelation function of R6G in 0.5Ac/0.3Ur/0.2Sor DES at different temperatures with single component diffusion model and anomalous diffusion model.

Temp (K)	τ_{1D}	$\tau_{anamolous}$	α
318	19043	17670	0.73
323	17838	16830	0.76
328	16500	16000	0.8
333	13345	12726	0.85
338	11992	11303	0.85
343	9671	9027	0.86

Section S11: Log-log plot and Arrhenius analysis of average translational diffusion (obtained using 1-D and anomalous fitting function) of 0.5Ac/0.3Ur/0.2Sor DES

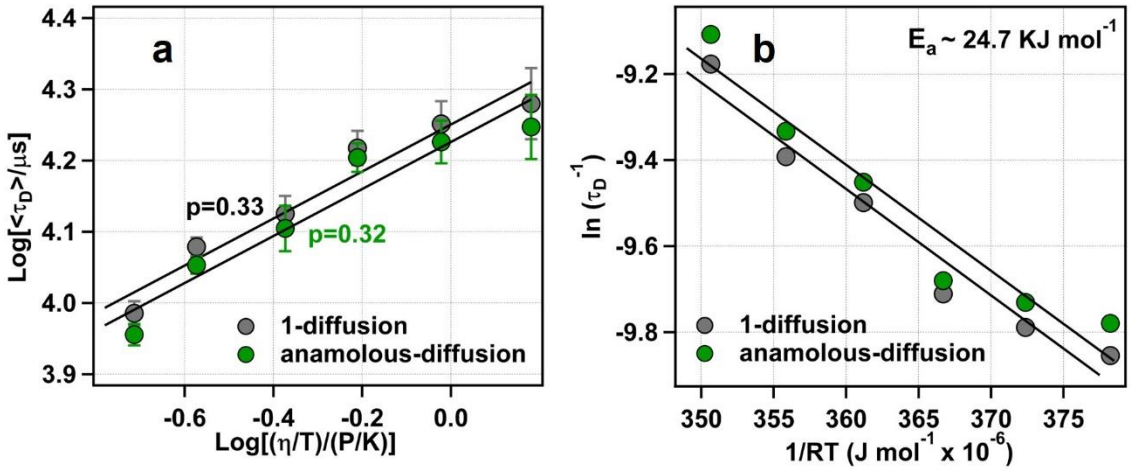

Figure S5: (a) log-log plot of average translational diffusion time of R6G in 0.5Ac/0.3Ur/0.2Sor DES (from fitting using 1-Diffusion and anomalous diffusion model) (τ_D) vs temperature reduced viscosity (η/T) with the linear fit represented by solid black line. (b) Arrhenius plot of average probe diffusion time obtained from two different fitting models.

Section S12: Temperature dependent time-resolved emission spectrum (TRES) of C153 in 0.55Ac/0.36Ur/0.09PEG DES

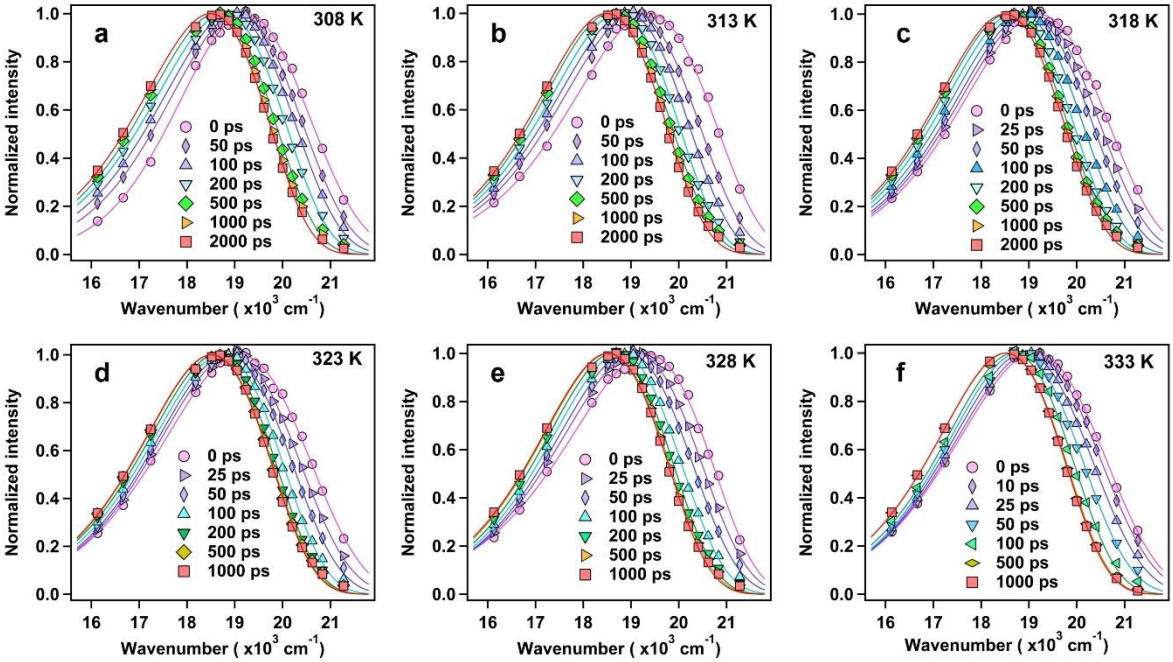

Figure S6: (a)Temperature dependent time-resolved emission spectrum. Emission spectrum at various times are colour-coded and mentioned in the respective plots. (c) Solvent response functions at different temperatures. Solid lines represent fitting by equation 3.

Section S13: Representative solvent response functions of 0.55Ac/0.36Ur/0.09PEG DES and Log-Log plot of average solvation time vs temperature reduced viscosity

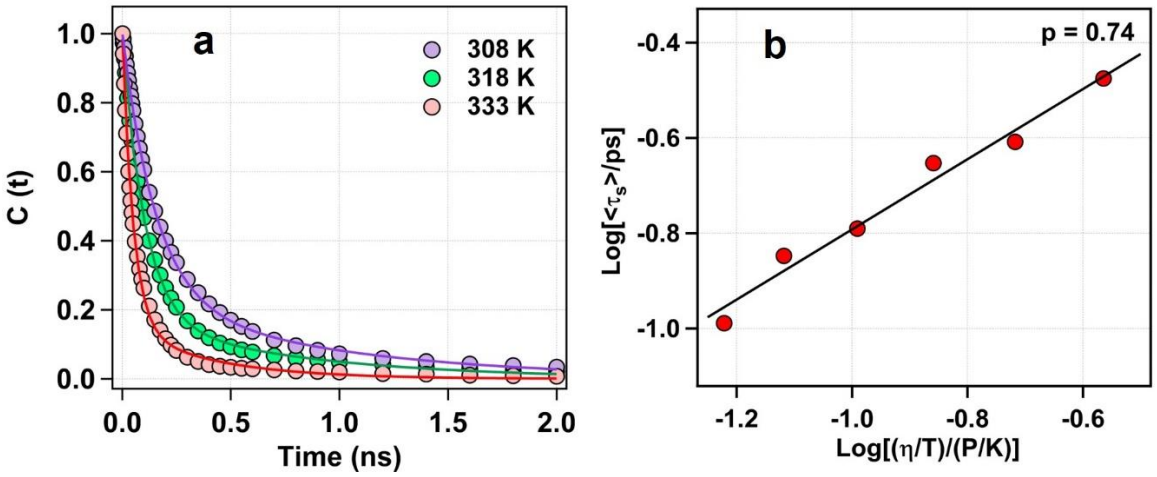

Figure S7: (a) Solvent response functions at three representative temperatures. Solid lines represent fitting by equation 3. (a) Log-Log plot of average solvation time $\langle \tau_s \rangle$ vs temperature reduced viscosity, $\left(\frac{\eta}{T}\right)$, with a linear fit (solid black line).

Section S14: Biexponential fitting parameters of solvent response function S(t) of 0.55Ac/0.36Ur/0.09PEG DES

Table S5: Biexponential fitting parameters of solvent response function S(t) of 0.55Ac/0.36Ur/0.09PEG DES and its viscosity at different temperatures.

Temp (K)	b_1	τ_{S1} **(ps)**	b_2	τ_{S2} **(ps)**	$\langle\tau_S\rangle$ **(ps)**
318	0.76	151	0.24	920	335
323	0.80	101	0.20	820	246
328	0.82	102	0.18	780	222
333	0.86	78	0.14	700	162
338	0.87	67	0.13	660	142
343	0.85	50	0.15	400	103

Section S15: Raw data of Dielectric measurement of 0.5Ac/0.3Ur/0.2Sor DES with cole-cole fitting

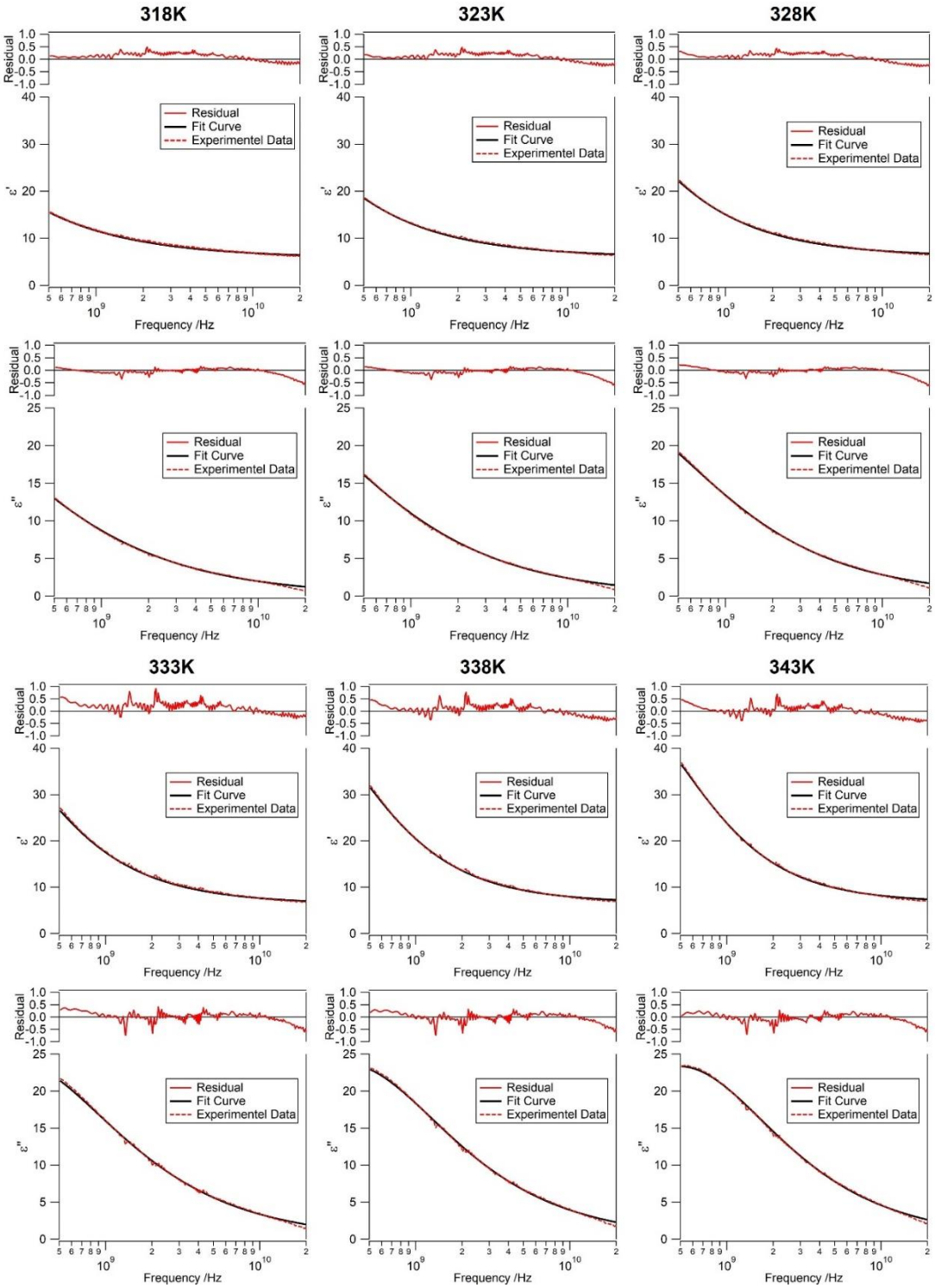

Figure S8. Fitting of real (ε') and imaginary (ε'') part of the complex dielectric spectra of 0.5Ac/0.3Ur/0.2Sor DES at different temperatures with cole-cole (equation 2 when $\alpha = 1$, $0< \beta < 1$ and β is interpreted a distribution of the relaxation time). Upper panel for each temperature represents the real part whereas lower is the imaginary part.

Section S16: Fitting parameters of dielectric relaxation data with cole-cole fitting function for 0.5Ac/0.3Ur/0.2Sor DES

Temperature (K)	$\Delta\varepsilon_1$	τ_1(ns)	β	ε_∞
318	96.26	3.710	0.684	5.72
323	82.38	1.800	0.721	5.88
328	74.04	1.040	0.753	6.02
333	68.85	0.665	0.781	6.23
338	64.27	0.450	0.808	6.44
343	61.19	0.325	0.830	6.54

Section S17: Temperature dependent value of β for all the acetamide base non-ionic DES

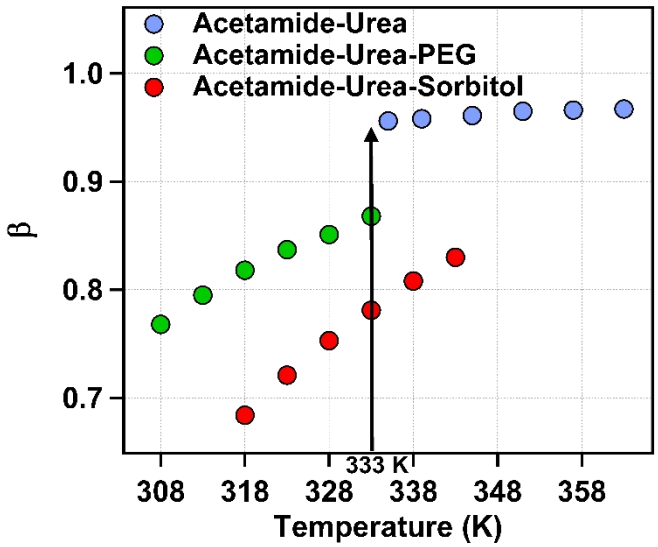

Figure S9. Temperature dependent value of β for all the acetamide base non-ionic DES.

Section S18: Translational dynamics of R6G in 0.55Ac/0.36Ur/0.09PEG DES via single molecular level FCS

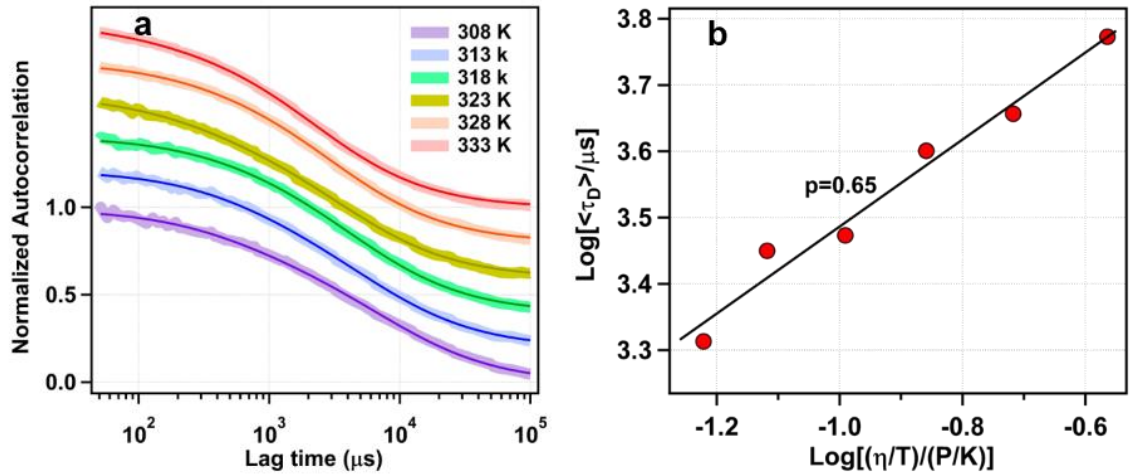

Figure S10: (a) Translational dynamics via single molecular level FCS. Normalized fluorescence intensity autocorrelation curve of R6G in 0.55Ac/0.36Ur/0.09PEG DES at different temperatures. Fitting lines are shown by solid lines. (b) log-log plot of average translational diffusion time (τ_D) vs temperature reduced viscosity (η/T) with the linear fit represented by solid black line.

Section S19: Fitting parameter of fluorescence intensity autocorrelation function of R6G in 0.55Ac/0.36Ur/0.09PEG DES

Table S6: Fitting parameter of fluorescence intensity autocorrelation function of R6G in 0.55Ac/0.36Ur/0.09PEG DES at different temperatures with two component diffusion model.

Temperature (K)	τ_{D1} (μs)	N_1	τ_{D2} (μs)	N_2	$\langle\tau_D\rangle$ (μs)
308	0.34	0.67	687	8585	5926
313	0.33	0.66	811	6396	4534
318	0.22	0.77	662	4937	3987
323	0.28	0.68	339	4056	2972
328	0.18	0.79	400	3368	2817
333	0.14	0.8	150	2390	2056

References:

1. N. Das and P. Sen, *The Journal of Physical Chemistry B*, 2020, **124**, 5858-5871.
2. T. Wohland, S. Maiti and R. Macháň, *An introduction to fluorescence correlation spectroscopy*, IOP Publishing2020.
3. J. R. Lakowicz, *Principles of fluorescence spectroscopy*, Springer2006.